Palaeoceanographic and environmental changes in the eastern Fram Strait during the last 14,000 years based on benthic and planktonic foraminifera

Chiara Consolaro[1,2], Tine L. Rasmussen[1] and Giuliana Panieri[1]

[1]{**CAGE** - Centre for Arctic Gas Hydrate, Environment and Climate, Department of Geosciences, UiT the Arctic University of Norway, Dramsveien 201, N-9037 Tromsø, Norway}

[2]{School of Geography, Earth and Environmental Sciences, Plymouth University, Drake Circus, Plymouth PL4 8AA, United Kingdom}

Correspondence to: C. Consolaro (chiara.consolaro@plymouth.ac.uk; chiara.consolaro@icloud.com)

Abstract

Benthic and planktonic foraminifera, stable isotopes and other geochemical and sedimentological parameters have been investigated in a sediment core from Vestnesa Ridge (79°N, NW Svalbard margin, 1300 m water depth) in order to reconstruct the palaeoceanographic and palaeoenvironmental evolution of the eastern Fram Strait during the last 14,000 years. Our multiproxy data and, in particular, our high-resolution benthic foraminiferal record allow a detailed reconstruction of the intermediate water flow in the eastern Fram Strait. During the Bølling-Allerød warm interstadials the high proportion of the benthic Atlantic species *Cassidulina neoteretis* suggests the presence of chilled Atlantic-derived water at the bottom of the Vestnesa Ridge, while the dominance of the polar planktonic species *Neogloboquadrina pachyderma* (s) indicates cold polar surface conditions.

During the Younger Dryas cold stadial the inflow of Atlantic-derived water was weakened and of lower temperature compared to the previous interval, as suggested by the increase in the glacio-marine indicator *Cassidulina reniforme* and the lower percentages of *C. neoteretis*. After 11,000 cal yrs BP the abrupt increase in relative abundance of the benthic species *Cibicides wuellerstorfi* and *Oridorsalis umbonatus*, indicates a shift to interglacial conditions with deep convection and generation of cold intermediate water. Warm surface water conditions were finally established at about 10,300 cal yrs BP, when *Turborotalita quinqueloba* became the dominant planktonic species. Generally warmer conditions than today were recorded in the middle Holocene, with a mild cooling at about 8200 cal yrs BP and a more pronounced cool interval with an abrupt decrease in *T. quinqueloba* between 7000 and 6200 cal yrs BP. Cold climatic conditions were established around 4100 cal yrs BP when *N. pachyderma* (s) became again the dominant species and the polar benthic species *Cribroelphidium excavatum* appeared.

1 Introduction

The Fram Strait is the only deep-water gateway to the Arctic, where water masses between the Atlantic and the Arctic Ocean can exchange. Two main surface currents dominate the Fram Strait: warm Atlantic Water to the east and cold polar water to the west (Aagaard et al., 1987). Here we present data from sediment core JM10-330GC from the Vestnesa Ridge, eastern Fram Strait. The core site is located under the flow of Atlantic Water in the vicinity of the Arctic Front (Fig. 1), which makes it an ideal location for a detailed reconstruction of the distribution of Atlantic Water and oceanic fronts at high latitude in the past. Several studies have reconstructed climatic and environmental changes of the eastern Fram Strait and western Svalbard margin covering the last deglaciation and the Holocene (e.g., Hald et al., 2004; Ebbesen et al., 2007; Rasmussen et al., 2007; Müller et al., 2009; Werner et al., 2013; 2016; Zamelczyk et al., 2012; Aagaard-Sørensen et al., 2014a, b), but mostly with proxies for surface water conditions. Only a few have presented records of benthic foraminiferal distribution patterns. Benthic foraminifera are indicators of the amount and quality of food reaching the seafloor as well as bottom currents, water mass properties and sedimentary conditions (e.g., Gooday, 1988; Murgese and de Decker, 2005; Murray, 2006 and references therein; Jorissen et al., 2007; Rasmussen and Thomsen, 2017). Here we present a detailed micropalaeontological investigation based on the distribution patterns of benthic and planktonic foraminifera, together with sedimentological and geochemical data, in order to reconstruct the palaeoceanographic and palaeoenvironmental evolution of the eastern Fram Strait during the last 14,000 years.

2 Study area

2.1 Geological setting

The study area is the Vestnesa Ridge, an elongated sediment drift offshore the western Svalbard margin at about 79°N in the eastern Fram Strait (Figs 1, 2a). The crest of the Vestnesa Ridge is perforated by pockmarks (Vogt et al., 1994; Hustoft et al., 2009; Fig. 2b), where seepage of gas and fluids occurs or has occurred (Judd and Hovland, 2007). Active venting has recently been observed on the eastern part of the ridge as acoustic gas flares (Hustoft et al., 2009; Bünz et al., 2012). Sediment core JM10-330GC has been retrieved from the deeper (ca. 1300 m water depth), western part of the ridge within a presently inactive pockmark (Bünz et al., 2012; Consolaro et al., 2015) (Fig. 2b).

2.2 Modern oceanographic setting

Two main surface currents dominate the Fram Strait: the northward flowing West Spitsbergen Current (WSC) to the east and the southward flowing East Greenland Current (EGC) to the west (Aagaard et al., 1987) (Fig. 1). The relatively warm and saline WSC (T >2°C and S >35 PSU; Hopkins 1991) is the northern branch of the North Atlantic Current (NAC). The WSC is the major source of heat and salt to high northern latitudes, and contributes to the generation of deep waters in the Nordic Seas (Aagaard et al., 1985).

Conductivity-Temperature-Depth (CTD; Fig. 3) data collected in June 2010 near the coring site (Fig. 2b) show the relatively warm and salty Atlantic Water (AW) underneath a thin, mixed layer of surface water of low salinity. The AW overlies the Greenland Sea Intermediate Water (GSIW), which is generated from convection in the Nordic Seas and represents one of the deeper components of the WSC (Aagaard et al., 1987). Cold, less saline and ice-loaded polar water (T 0-2°C, S 33–34.4 PSU; Hopkins, 1991) is transported southwards in the western Fram Strait along the East Greenland coast into the North Atlantic Ocean by the

EGC, and into the Barents Sea by the East Spitsbergen Current (ESC) (Fig. 1). Where polar water and Atlantic Water meet they mix and form Arctic water masses (T ~ 0.5°C, S ~34.8 PSU; Hopkins, 1991) characterised by seasonal sea-ice cover. The difference in temperature, salinity and sea-ice cover between the three main surface water masses creates steep climatic gradients: the Arctic Front between Arctic and Atlantic Waters and the Polar Front between polar and Arctic water masses (Hopkins, 1991). The Arctic Front is associated with the maximum extension of the sea-ice margin in winter, while the Polar Front corresponds to the average summer sea-ice margin (Vinje, 1977; NSIDC data, 2016) (Fig. 1). The area between the two fronts defines the marginal ice zone (MIZ), an area with very high seasonal productivity (Smith et al., 1987; Gradinger and Baumann, 1991; Hirche et al., 1991). The seasonal ice retreat and associated primary production is strictly dependent on the strength and temperature of the inflowing Atlantic Water (e.g., Knies et al., 1999, 2000; Nørgaard-Pedersen et al., 2003; Wollenburg et al., 2004). The outer Vestnesa Ridge area is now free of sea ice during most of the year, but is still close to the modern winter ice margin (Fig. 1) (NSIDC data, 2016).

3 Material and methods

Gravity core JM10-330GC (79.13°N, 5.6°E; 420 cm long) was retrieved during a cruise with the RV *Jan Mayen* (now RV *Helmer Hanssen*) in June 2010, from 1297 m water depth (mwd) at a pockmark located on the western part of the Vestnesa Ridge (Figs 1, 2). The handling and sampling procedures for JM10-330GC have already been described by Consolaro et al. (2015). Visual inspection and X-ray images revealed no disturbances from or evidence of presence of gas. The colour scan images of the core, together with the lithological log, the

magnetic susceptibility, the concentration of IRD >1 mm and the sedimentation rate have been published previously by Consolaro et al. (2015).

The samples were collected in 1-cm slices every 5 cm, freeze-dried, weighed, wet-sieved over mesh sizes of 63 μm, 100 μm, and 1 mm, dried at 40°C and weighed again. Eighty-five samples were analysed giving an average time resolution of 165 years. Mineral grains, biogenic silica remains (diatoms, radiolarians and sponge spicules) and pyritized burrows were counted in the 100–1000 μm size fraction.

The weight percentages (wt%) of total carbon (TC), total organic carbon (TOC) and calcium carbonate ($CaCO_3$) were determined every 5 cm. TC and TOC were measured from bulk samples using a Leco CS-200 induction furnace. TC was measured directly on the dried and crushed samples, while TOC was measured after the inorganic carbon was removed with HCl (10%) at room temperature. The $CaCO_3$ content (wt%) was calculated using the equation of Espitalié et al. (1977):

$$CaCO_3 = (TC - TOC) \times 100 / 12$$

Oxygen and carbon isotope data measured on the planktonic foraminiferal species *Neogloboquadrina pachyderma* sinistral (s) and the benthic species *Cassidulina neoteretis* have been previously published by Consolaro et al. (2015), while the isotope data generated using *Cibicides wuellerstorfi* are new (Supplementary Table S1). Stable isotope analyses were carried out at the Leibniz-Laboratory for Radiometric Dating and Isotope Research in Kiel, Germany, using a Finnigan MAT-253 mass spectrometer with Kiel IV system (analytical precision of ±0.05‰ for $\delta^{13}C$ and ±0.1‰ for $\delta^{18}O$ estimated by certified standard NBS-19). Isotope results are reported in standard delta notation relative to Vienna Peedee Belemnite (VPDB). The $\delta^{18}O$ isotopic values were corrected for ice volume effect ($\delta^{18}O_{IVC}$) with a correction of 0.11‰ $\delta^{18}O$ per ten meters sea level change (Fairbanks, 1989). The values

obtained for *C. wuellerstorfi* were corrected for disequilibrium with seawater by adding 0.64 ‰ (Duplessy et al., 1980).

For this study, benthic and planktonic foraminifera were picked from the 100 μm to 1 mm size fraction, counted and identified to species level following the guidelines from Knudsen (1998). A minimum of 300 benthic and 300 planktonic foraminifera specimens were counted for each sample. When necessary, the residues were split and the total number of foraminifera calculated. In the lower part of the record (between 420 and 280 cm) one sample for planktonic and eight samples for benthic foraminifera contained between 150 and 270 specimens. These data were, therefore, treated with caution but they were still included in the calculations for relative and absolute abundances (Supplementary Table S2). The taxonomy employed follows Loeblich and Tappan (1987). According to Darling et al. (2006), if the percentage of right coiling *Neogloboquadrina pachyderma* at high-latitudes is less than 3%, they should be considered as aberrant morphotypes of *N. pachyderma* sinistral (s) and should be referred to as *N. pachyderma* dextral (d). Since the percentage of right-coiling specimens in our sediment samples is close to 3% (lower in the early part of the record and slightly higher during the Holocene), we decided not to distinguish *N. pachyderma* (d) from *N. incompta* and named all the right coiling specimens as *N. pachyderma* (d).

Relative abundance (%) and flux (no. specimens/cm^2/yr) of the most abundant species were calculated for each sample (Supplementary Table S2). Percentages of the planktonic species *N. pachyderma* (s) and *Turborotalita quinqueloba* have been published previously by Consolaro et al. (2015). Flux, or foraminiferal accumulation rates, were calculated using the formula of Ehrmann and Thiede (1985):

Flux (#/cm^2/yr) = (absolute abundance (#/g) x dry bulk density (g/cm^3) x SAR (cm/ka))/1000,

where # is the number of foraminiferal specimens, and SAR is the sediment accumulation rate. Dry bulk density was calculated based on sediment water content and wet bulk density, acquired by GEOTEK multisensor core logging.

The age model has been published by Consolaro et al. (2015) and is based on eight AMS-^{14}C dates. In the following, ages are presented as cal yrs BP or cal kyrs BP.

4 Results

The record of core JM10-330GC is subdivided into five time intervals based on the age model, the benthic and planktonic foraminiferal distribution, the lithological features and the stable isotope records (Figs 4–7). The first interval coincides with the upper part of the Bølling interstadial and the Allerød interstadial (from the base of the core at 14,120 to 12,850 cal yrs BP). The second interval corresponds to the Younger Dryas (YD) stadial (12,850–11,650 cal yrs BP) and is characterised by a greenish-grey, sandy layer at the base (12,700–12,500 cal yrs BP). The early Holocene interval starts at 11,650 cal yrs BP and consists of fine-grained, silty clay with high concentration of biogenic siliceous remains, especially diatoms (*Coscinodiscus* spp.), termed diatom-rich mud (11,100–8800 cal yrs BP). The middle Holocene interval is defined by high % of *T. quinqueloba* and low % of *N. pachyderma* (s) (8800–4100 cal yrs BP). The late Holocene is defined by the presence of the benthic foraminiferal species *Cribroelphidium excavatum* and high relative abundance of *N. pachyderma* (s) from 4100 to 150 cal yrs BP (age of the top of the core). More details about the stratigraphy of the core JM10-330GC, including the sandy layer and the diatom-rich layer, can be found in Consolaro et al. (2015).

178 **4.1 Stable isotope analysis**

179 Stable isotope analyses ($\delta^{18}O$ and $\delta^{13}C$) of the planktonic foraminifera *N. pachyderma* (s) and
180 the infaunal benthic foraminifera *C. neoteretis* (Fig. 5) have been previously published in
181 Consolaro et al. (2015). Their $\delta^{13}C$ records show two Carbon Isotope Excursions (CIEs)
182 attributed to influence by seeping gas (for details see Consolaro et al., 2015). Excluding the
183 CIE events, both $\delta^{13}C$ records present low values in the Younger Dryas and in the early
184 Holocene (Fig. 5). The new Holocene $\delta^{13}C$ record of *C. wuellerstorfi* shows low values in the
185 early Holocene with two negative peaks at 11,000 and 10,000 cal yrs BP, while in the middle
186 and late Holocene the values are generally higher, with small negative peaks at 8800 and 8000
187 cal yrs BP and a gradual decrease in the last 3000 years (Fig. 5). The $\delta^{18}O$ record of *C.*
188 *wuellerstorfi* shows relatively high values in the diatom-rich layer, and peaks of high values
189 around 8000 and 4500 cal yrs BP (Fig. 5).

190

191 **4.2 Foraminiferal abundance and distribution**

192 The planktonic foraminifera assemblage is dominated by two species: *Neogloboquadrina*
193 *pachyderma* (s) (mean value 55%) and *Turborotalita quinqueloba* (mean value 40%) (Fig. 6).
194 Other less abundant species are *N. pachyderma* (d), *Globigerinita uvula*, *Globigerinita*
195 *glutinata* and *Globigerina bulloides*. Before 10,800 cal yrs BP *N. pachyderma* (s) dominates
196 the assemblage with *T. quinqueloba* as a minor component. After 10,300 cal yrs BP, in the
197 early and middle Holocene, *T. quinqueloba* dominates the assemblage. The percentage of *N.*
198 *pachyderma* (s) shows a gradual increase starting at about 4900 cal yrs BP. The number of
199 planktonic foraminifera per gram of dry sediment and the total flux of planktonic foraminifera
200 show similar trends with very low abundance in the lower part of the record, with the

exception of the sandy layer at 12,700 cal yrs BP, and a sharp increase at about 9800 cal yrs BP (Fig. 6g).

A total number of 73 benthic species were found (Appendix). The most abundant species are: *Cassidulina neoteretis, Cassidulina reniforme, Melonis barleeanus, Lobatula lobatula, Cibicides wuellerstorfi, Epistominella arctica, Cribroelphidium excavatum, Oridorsalis umbonatus, Ioanella tumidula, Stainforthia loeblichi, Nonionella iridea*, and *Nonionellina labradorica* (Fig. 7). *Cassidulina neoteretis* dominates in the Bølling-Allerød interstadials (Fig. 7a). The sandy layer at about 12,700 cal yrs BP, contains an assemblage with dominance of *M. barleeanus*, *O. umbonatus* and *I. tumidula*, while just above *S. loeblichi* and *N. iridea* show major peaks (see discussion in section 5.2) (Fig. 7c, h–k). The diatom-rich layer (11,100−8800 cal yrs BP) is dominated by *Cassidulina reniforme* together with *Cibicides wuellerstorfi*, *M. barleeanus* and *Oridorsalis umbonatus*, with *Epistominella arctica* as a minor component (Fig. 7). After 4100 cal yrs BP *C. wuellerstorfi* and *E. arctica* show a decrease in their relative abundance and *Cribroelphidium excavatum* appears (Fig. 7g). The number of benthic foraminifera per gram dry sediment and the total flux of benthic foramnifera present low values in the deglacial part of the record and gradually increase after 11,000 cal yrs BP (Fig. 7p).

5 Reconstruction of palaeoceanographic and palaeoenvironmental conditions in the last 14,000 years

5.1 Upper part of Bølling and Allerød interstadials (14,120–12,850 cal yrs BP): cold surface water conditions with Atlantic-derived water at the bottom

The Bølling and Allerød interstadials (B-A) are described as warm periods in northern Europe and from the start of the Bølling period (14,650–14,025 cal yrs BP), the Svalbard-Barents Sea ice sheet retreated rapidly (e.g., Vorren and Kristoffersen, 1986; Mangerud et al., 1992; Lubinski et al., 2001). The oldest sediments in core JM10-330GC contain a relatively high concentration of sand (>63 μm) and IRD (>100 μm and >1 mm) deposited rapidly and indicating unstable climatic conditions characterised by melting and re-advancing phases of glaciers and sea-ice, as also described by e.g., Landvik et al. (1998) (Fig. 4a, c). Low values of planktonic and benthic foraminifera total flux can indicate low primary productivity (Figs 6g, 7p) supported by low $\%CaCO_3$ (Fig. 4e). The presence of aragonitic pteropods indicates good preservation, as aragonite is more vulnerable to dissolution than calcite (e.g., Cherns and Wright, 2009) (Fig. 6h). The dominance of the polar planktonic foraminiferal species *N. pachyderma* (s) (mean value 90%; Fig. 6a) indicates polar conditions and presence of cold Arctic and polar surface water (Table 1). This is supported by the high planktonic $\delta^{18}O_{IVC}$ values that also indicate cold conditions at the subsurface (Fig. 5). Similar assemblages with very high relative abundance of *N. pachyderma* (s) and low planktonic flux have previously been reported during the B-A from the western Svalbard margin (Ebbesen et al., 2007; Rasmussen et al., 2007; Aagaard-Sørensen et al., 2014a; Fig. 8) and the south-western Barents Sea (Sarnthein et al., 2003; Aagaard-Sørensen et al., 2010).

The benthic foraminiferal assemblage is dominated by *C. neoteretis* (mean value 55%), which indicates the presence of chilled Atlantic-derived Water (Table 1) (Fig. 7a). Such high relative abundance of *C. neoteretis* occurs in the modern sediments of the Barents and Kara seas in areas with subsurface inflow of Atlantic Water below a layer of polar water at the surface

(Lubinski et al., 2001). It is also common in sediments overlain by Atlantic Intermediate Water in Greenland fjords (Jennings and Weiner, 1996; Jennings et al., 2006) and in the Arctic Ocean (Wollenburg and Mackensen, 1998). The very high proportion of *C. neoteretis* during the B-A suggests a very strong inflow of chilled Atlantic-derived water at the bottom. Similar conditions, based on a high proportion of *C. neoteretis*, have been suggested by Lubinski et al. (2001) for the same time interval in the northern Barents Sea. *Melonis barleeanus* is the second most abundant species during the B-A (22%; Fig. 7c) possibly indicating high sedimentation rates with steady food supply (Table 1), and it has been associated with the presence of Atlantic-derived water in the Arctic (Polyak et al., 2002). Less abundant species are *C. reniforme* (11%; Fig. 7b), an Arctic species common in cooled Atlantic Water and in glacio-marine environments (Table 1), and *Lobatula lobatula* (4%; Fig. 7d), an indicator of strong bottom current activity (Table 1).

Our reconstruction (Fig. 10) agrees well with previous findings from the Western Svalbard margin (Rasmussen et al., 2007; Ślubowska-Woldengen et al., 2007; Aagaard-Sørensen et al., 2014a), the northern Svalbard margin (Koç et al., 2002; Ślubowska et al., 2005), the marginal Arctic Ocean (Wollenburg et al., 2004) and the northern Barents Sea (Polyak and Solheim, 1994; Lubinski et al., 1996, 2001; Klitgaard-Kristensen et al., 2013), where Atlantic Water was found to be continuously present below polar surface water from the Bølling interstadial onwards.

5.2 Younger Dryas stadial (12,850–11,650 cal yrs BP): a not very cold interval with a sandy layer associated with a meltwater event

The low planktonic and benthic $\delta^{18}O$ values during the YD correlating with the deposition of the sandy layer are most likely the result of reduced salinity due to a local meltwater event

(Fig. 5). Similar short local melt water pulses during the YD have previously been recorded from Storfjorden Trough (Rasmussen et al., 2007), central (Zamelczyk et al., 2012) and western Fram Strait (Bauch et al., 2001), and eastern Greenland shelf (Jennings et al., 2006). A slight decrease in sand (>63 μm) and IRD (>100 μm and >1 mm) with lower sedimentation rate above the sandy layer (Fig. 4), can probably be linked to increased sea-ice cover and reduced iceberg transport, as previously documented on the western and northern Svalbard margin (Koç et al., 2002; Wollenburg et al., 2004; Ebbesen et al., 2007; Ślubowska-Woldengen et al. 2007; Aagaard-Sørenesen et al., 2014a).

During the Younger Dryas the total flux and concentration of planktonic foraminifera was very low, except in the sandy layer, indicating, together with the low $CaCO_3$ content, a very low productivity (Figs 4e, 6g). The planktonic assemblage was still dominated by *N. pachyderma* (s), but with slightly lower mean values (86%) compared to the Bølling-Allerød interstadials, indicating slightly less severe conditions (Fig. 6a). Similar surface conditions were also found in records from the western Svalbard margin (Ebbesen et al., 2007; Rasmussen et al. 2007; Aagaard-Sørenesen et al., 2014a; Fig. 8).

The total flux and concentration of benthic foraminifera show here the lowest values of the record, except in the sandy layer (Fig. 7p), confirming that the low productivity also affected the deep benthic community. Before, and during, the deposition of the sandy layer the high relative abundance of *M. barleeanus* (Fig. 7c) and the presence of *L. lobatula* (Fig. 7d) indicate high sedimentation rates and strong current activity, while the peaks of *Oridorsalis umbonatus* and *Ioanella tumidula* (Fig. 7h-i) can indicate oligotrophic conditions (Table 1), as also suggested by the very low values of TOC registered during the event (Fig. 4e). The organic-rich top part of the sandy layer was colonised by the opportunistic species *Nonionella iridea* and *Stainforthia loeblichi* (Table 1). These two species probably were able to exploit

294 the high organic content in the sediment (Fig. 7k, j; Table 1). Above the sandy layer the TOC
295 values increase, possibly indicating a progressive eutrophication of the ecosystem (Fig. 4e).
296 Increased TOC and marine biomarker values during the late YD have been reported in the
297 Fram Strait/Yermak Plateau (Birgel and Hass, 2004; Müller and Stein, 2014). After the melt
298 water event the benthic assemblage is characterised by high percentages of the glacio-marine
299 indicator *C. reniforme* with lower percentages of *C. neoteretis*, *M. barleeanus* and *L. lobatula*
300 (Fig. 7a–d). This assemblage suggests reduced influence of Atlantic Water and increased
301 influence of colder bottom water with weaker current activity (Fig. 10).

302 The YD cold period is not particularly conspicuous in our data (Fig. 10). The sea surface was
303 still influenced by cold polar water, but with open water conditions that allowed substantial
304 primary production, while the influx of Atlantic-derived Water at the bottom was weaker,
305 with low current velocity and probably of lower salinity (low $\delta^{18}O$ benthic values, Fig. 5).
306 The relatively low planktonic and benthic $\delta^{13}C$ values are an indication of poor ventilation
307 and probably strong stratification of the water column (Figs 5, 10). Similar low $\delta^{13}C$
308 planktonic values have been registered in other western Svalbard margin records during the
309 same interval (Ebbesen et al., 2007; Aagaard-Sørensen et al. 2014a; Fig. 9i, j). These data are
310 consistent with previous studies from the northern and western Svalbard margin that reported
311 seasonal open water conditions and reduced influence of Atlantic Water at the bottom (e.g.,
312 Ślubowska et al., 2005; Rasmussen et al., 2007; Ślubowska-Woldengen et al., 2007; Aagaard-
313 Sørensen et al. 2014a; Müller and Stein, 2014). Colder conditions with almost permanent ice
314 cover, very little Atlantic-derived water influence and low-abundance or foraminifera-barren
315 sediments, have been reported from the eastern Svalbard margin and the Barents Sea (Polyak
316 and Solheim, 1994; Hald et al., 1999; Lubinski et al., 2001; Aagaard-Sørensen et al. 2010;
317 Klitgaard et al., 2013).

318

319 **5.3 Early Holocene (11,650–8800 cal yrs BP): unstable with shift to stable interglacial**
320 **conditions around 11,000 cal yrs BP in the benthic environment and delayed**
321 **warming in the planktonic environment**

322 The transition from the YD to the early Holocene is characterised by unstable conditions with
323 presence of IRD and high sedimentation rates reflecting increased sediment transport by
324 melting icebergs and/or sea ice (Fig. 4). Similar surface conditions have been recorded both
325 west and north of Svalbard during this period (Ebbesen et al., 2007; Ślubowska-Woldengen et
326 al., 2007; Aagaard-Sørensen et al., 2014a). In our record the early Holocene is marked by the
327 deposition of a thick (1.1 m) diatom-rich mud layer characterised by abundant *Coscinodiscus*
328 spp. in the 63–100 μm fraction and high abundance of radiolarian and sponge spicules in the
329 >100 μm fraction (Fig. 4d). Similar diatom-rich mud layers have been observed in the Fram
330 Strait further to the north of our site (Stabell, 1986), in the southern Norwegian Sea (Stabell,
331 1986; Koç-Karpuz and Jansen, 1992; Birks and Koç, 2002) and western Svalbard margin
332 (Jessen et al., 2010; Aagaard-Sørensen et al., 2014a). The diatom-rich layer is time
333 transgressive and has been attributed to the northward movement of the Polar Front (Jansen et
334 al., 1983; Stabell, 1986). It is considered a chronostratigraphic marker for the western
335 Svalbard slope with an early Holocene age (10,100−9840 cal yrs BP in core JM03-373PC,
336 Jessen et al., 2010; and 10,500−9800 cal yrs BP in core MSM5/5-712-2, Aagaard-Sørensen et
337 al., 2014a). In our record the diatom-rich layer is thicker and more expanded in time (11,100–
338 8800 cal yrs BP), possibly indicating prolonged influence of the marginal ice zone over outer
339 Vestnesa Ridge than in other records further south (Fig. 2).

340 In the early part of the early Holocene (11,650−10,800 cal yrs BP) the surface conditions
341 were still strongly influenced by cold polar water (71−75% of *N. pachyderma* (s); Fig. 6a).

Thereafter, a very unstable period occurred with strong fluctuations in the relative abundance of *N. pachyderma* (s) (from 26% to 82%) and *T. quinqueloba* (from 14% to 86%), until warm surface conditions were finally established around 10,300 cal yrs BP, when *T. quinqueloba* became the dominant species (Fig. 6a, b). Similar unstable conditions with fluctuating sea subsurface temperature (SST-100 m) have been observed in the neighbouring core MSM5/5-723-2 until 10,600 cal yrs BP (Werner et al., 2016), but with smaller amplitude in fluctuations of the planktonic assemblages (Fig. 8e). A similar pattern in the reconstructed SST based on Mg/Ca can be observed in core MSM5/5-712-2, but not in the faunal assemblage (Aagaard-Sørensen et al., 2014a; Fig. 8c). Further south in the Storfjord Trough strong fluctuations in the planktonic record are registered earlier between 11,600 and 11,000 cal yrs BP suggesting a 'Pre-Boreal Type' event (Rasmussen et al., 2007; Fig. 8a). Despite the differences between the records during the unstable transition from the YD to the Holocene, which might have been caused by local conditions, a common pattern with a clear shift to warmer surface/subsurface conditions occurs between 10,500 and 10,300 cal yrs BP in all records (Fig. 8; Ebbesen et al., 2007; Rasmussen et al., 2007; Aagaard-Sørensen et al., 2014a; Werner et al., 2016). The lowest peak in abundance and flux of *N. pachyderma* (s), together with a peak of *G. uvula* and a sharp increase in planktonic foraminiferal productivity at 9800 cal yrs BP, mark the beginning of Holocene optimum climatic conditions in our record (Fig. 6a, d, g). The pronounced peak of *G. uvula* between 10,000 and 9,500 cal yrs BP, is a common feature in records from the western Svalbard margin (Fig. 8; Ebbesen et al., 2007; Rasmussen et al., 2007; Aagaard-Sørensen et al., 2014a), and can indicate the presence of highly productive surface waters in proximity of the oceanic fronts (Table 1). The concomitant increase in abundance and flux of the relatively thermophile species *N. pachyderma* (d) and *G. bulloides* demonstrates a stronger influence of warm Atlantic Water (Fig. 6c, f), as already observed in the Nordic Seas (Risebrobakken et al., 2011) and in the neighbouring core MSM5/5-712-2

(Aagaard-Sørensen et al., 2014a). Maximum oceanic heat advection through northward transport of Atlantic Water around 10,000 cal yrs BP (Riesebrobakken et al., 2011) led to cessation of iceberg transport, as suggested by the absence of IRD after 10,000 cal yrs BP in our record (Fig. 4c) and in other records along the western Svalbard margin (Ebbesen et al., 2007; Rasmussen et al., 2007, 2014; Jessen et al., 2010; Aagaard-Sørensen et al., 2014a). The planktonic $\delta^{18}O$ record shows first warming signals at about 10,300 cal yrs BP and minimum values around 9600 cal yrs BP (Figs 5, 10). A similar pattern with minimum $\delta^{18}O$ values after 10,000 cal yrs BP has been observed in the neighbouring cores MSM5/5-712-2 and MSM5/5-723-2 (Aagaard-Sørensen et al., 2014a; Werner et al., 2016; Fig. 9f, h) confirming warm climatic conditions and maximum Atlantic Water advection in the area during this time (Werner et al., 2016). Holocene climatic optimum conditions with higher SST than present have been reported in the western Fram Strait (Bauch et al., 2001), western Svalbard margin (Ebbesen et al., 2007; Hald et al., 2007; Aagaard-Sørensen et al., 2014a; Werner et al., 2016) and Barents Sea (Sarnthein et al., 2003; Berben et al., 2014) at about the same time. The northward heat transport gradually decreased after 10,000 cal yrs BP (Risebrobakken et al., 2011), but conditions warmer than today with high relative abundance of *T. quinqueloba* continued until about 8800 cal yrs BP (Ebbesen et al., 2007; Rasmussen et al., 2007; Aagaard-Sørensen et al., 2014a; Werner et al., 2016; Figs 8, 10).

The species composition of the benthic foraminiferal assemblages also shifted during the early Holocene (Fig. 7). In the beginning, the assemblage was still dominated by *C. reniforme*, *C. neoteretis* and *M. barleeanus*, but around 11,000-10,800 cal yrs BP, the increase in relative abundances of *C. wuellerstorfi* and *Oridorsalis umbonatus* indicate interglacial conditions similar to the modern environment on the Nordic Seas deeper slopes characterised by well oxygenated deep-waters (Table 1). The appearance of *Epistominella arctica*, an opportunistic phytodetritus feeder (Table 1), can indicate highly variable food productivity

during the deposition of the diatom-rich layer, as also shown by the high TOC values (Figs 7 and 4e). Cold deep-water conditions and decreased influence of Atlantic-derived water at the bottom is also indicated by the low proportion of *C. neoteretis* between 10,800 and 8200 cal yrs BP (Figs 7a, 10). Both benthic $\delta^{18}O$ records show relatively high values confirming cold bottom water conditions, with some signal of warming at 10,500 and 10,000 cal yrs BP, when the *C. neoteretis* record registers two minima (Fig. 5). Relatively low $\delta^{13}C$ values in *C. wuellerstorfi* have been observed around 11,000 and 10,000 cal yrs BP in our record (Figs 5, 9n, 10), and before 11,000 cal yrs BP in the neighbouring core MSM5/5-723-2 (Werner et al., 2016; Fig. 9o). Low epibenthic $\delta^{13}C$ values before 11,000 cal yrs BP have been reported in the Faroe-Shetland Channel by Risebrobakken et al. (2011), who argued that during the maximum of northward Atlantic Water advection some ^{13}C-depleted bottom waters up-welled affecting the planktonic $\delta^{13}C$ signal in the Nordic Seas. This would explain the low planktonic $\delta^{13}C$ values registered during the early Holocene in our record and in other records along the western Svalbard margin (Fig. 9i–l; Ebbesen et al., 2007; Aagaard-Sørensen et al., 2014a; Werner et al., 2016).

The shift towards interglacial conditions with the generation of cold intermediate water occurred around 11,000-10,800 cal yrs BP in the benthic environment, while warm surface water conditions finally established around 10,300 cal yrs BP (Fig. 10). Similar results with interglacial conditions established first in the benthic environment and a delayed appearance of Atlantic Water at the surface, has been described from the southwestern Svalbard margin (Rasmussen et al., 2007; Ślubowska-Woldengen et al., 2007).

5.4 Middle Holocene (8800–4100 cal yrs BP): warm conditions with a mild cooling around 8200 cal yrs BP and pronounced cooling between 7000 and 6200 cal yrs BP.

Warm climatic conditions with strong inflow of Atlantic Water at the surface lasted until about 7000 cal yrs BP, as indicated by the high relative abundance of *T. quinqueloba*, the presence of subpolar species and the high concentration and flux of planktonic foraminifera (Figs 6, 10). In contrast to neighbouring cores MSM5/5-712-2 and MSM5/5-723-2, where the '8200 cal yrs BP' climate anomaly is indicated by pronounced shifts in surface and deep-water proxy records (Werner et al., 2013, 2016), we see only a slight increase in flux and relative abundance of *N. pachyderma* (s) (Figs 6a, 8n), two higher peaks in $\delta^{18}O$ values and a $\delta^{13}C$ minimum in *C. wuellerstorfi* around 8000 cal yrs BP (Figs 5, 9b, n). This could indicate colder conditions and reduced deep-water ventilation, respectively.

A short episode with increased abundance of *N. pachyderma* (s) at the expense of *T. quinqueloba*, and with low planktonic foraminiferal concentration, occurred between 7000 and 6200 cal yrs BP (Figs 6, 8, 9, 10). Temperature lows at about 6900 and 6100 cal yrs BP (Fig. 8c) have been described in core MSM5/5-712-2 (Werner et al., 2013; Aagaard-Sørensen et al., 2014b) and, less pronounced, in core MSM5/5-723-2 (Werner et al., 2016; Fig. 8e). These cooling events have been linked to advances and retreats of the sea-ice margin connected to the movement of the Arctic Front (Werner et al., 2013). A general cooling trend from about 7000 cal yrs BP has been observed in several other records in the Nordic Seas (Sarnthein et al., 2003; Knudsen et al., 2004; Hald et al., 2007; Rasmussen et al., 2007) caused by reduced northward advection of Atlantic Water and cooling of the surface water (Hald et al., 2007; Risebrobakken et al., 2011). This cooling is also seen in our core (Fig. 5) and in general over the western Svalbard margin at about the same time (Ebbesen et al., 2007;

Rasmussen et al., 2007, 2014; Werner et al., 2013; 2016; Aagaard-Sørensen et al., 2014b; Fig. 9h–l).

After 6200 cal yrs BP *T. quinqueloba* returns to being the dominant species, although with lower relative abundance compared to the Holocene climatic optimum interval (Figs 6b, 8m). Subpolar species are present and together with the high concentration of planktonic foraminifera can indicate a fairly strong inflow of Atlantic Water and proximity to the oceanic fronts until about 4100 cal yrs BP (Fig. 10). A Similarly high proportion of *T. quinqueloba* has been described in core MSM5/5-712-2 (Werner et al., 2013; Fig. 8j) and in core MSM5/5-723-2 (although with lower abundance; Werner et al., 2016; Fig. 8p). These high relative abundances of *T. quinqueloba* differs from most other studies in the region (e.g., Bauch et al., 2001; Sarnthein et al., 2003; Ebbesen et al., 2007; Hald et al., 2007; Rasmussen et al., 2007; Risebrobakken et al., 2010), and can be attributed to a closer location of the core site to the Arctic Front compared to other studies, or to a better preservation of the more delicate *T. quinqueloba* shells. Similar results have been reported from Kveithola Trough in the western Barents Sea (Berben et al., 2014).

In the benthic environment, *C. wuellerstorfi* has a lower relative abundance than in the early Holocene (around 12%), while the opportunistic species *E. arctica* (10%) together with *M. barleeanus* (7%) and the phytodetritus feeders *Nonionella iridea* (5.8%) increase, pointing to more variable seasonal productivity and proximity to the oceanic fronts (Table 1), as also indicated by the high TOC values (Fig. 4e). The decrease in percentage of *O. umbonatus* towards the end of the time interval and the appearance of *N. labradorica* at the same time, also suggests an increase in productivity (Table 1). Generally high benthic $\delta^{13}C$ values can indicate stronger ventilation and deep-sea convection that, together with the increasing trend of the $\delta^{13}C$ in the planktonic record, also suggest a general increase in productivity (Figs. 5,

462 10), as already described in other records of the western Svalbard margin (Ebbesen et al.,
463 2007; Werner et al., 2013; 2016; Fig. 9i–o).

464 During the 8200 and the 7000–6200 cal yrs BP events only a small decrease in the relative
465 abundance of *C. wuellerstorfi* can be noticed (Fig. 5), suggesting that these cooling events
466 were more pronounced in the planktonic environment (see discussion above).

467

468 **5.5 Late Holocene (4100–150 cal yrs BP): a general cooling trend and a small warming**
469 **in the last 2000 years**

470 *Neogloboquadrina pachyderma* (s) becomes dominant again in the late Holocene interval,
471 showing a cooling trend started at about 4900 cal yrs BP (Figs 6a, 10). A similar, but more
472 abrupt climate shift occurred around 5200 cal yrs BP in core MSM5/5-712-2 (Werner et al.,
473 2013; Fig. 8c) and more gradually from 5000 cal yrs BP in core MSM5/5-723-2 (Werner et
474 al., 2016; Fig. 8e), showing a common cooling trend culminating with minimum temperatures
475 between 4000 and 3000 cal yrs BP (Werner et al., 2013; 2016; Aagaard-Sørensen et al.,
476 2014b). Increasing planktonic $\delta^{18}O$ values from about 5000 to 3000 cal yrs BP in our record
477 (Figs 5, 10) and in other records from the western Svalbard margin (Fig. 9h−l; Ebbesen et al.,
478 2007; Rasmussen et al., 2007; Werner al., 2013; 2016; Aagaard-Sørensen et al., 2014b) reflect
479 colder subsurface conditions in the whole area, while increased sea-ice biomarker
480 concentration indicates more severe sea-ice conditions (Müller et al., 2012; Werner et al.,
481 2013). A cooling trend with spreading of polar conditions associated with the so-called
482 Neoglacial starting at about 4000 cal yrs BP has also been reported south of Svalbard and in
483 Svalbard fjords (Sarnthein et al., 2003; Hald et al., 2004, 2007; Rasmussen et al., 2012). The
484 advance of the Polar Front and spreading of polar water caused the disappearance of
485 planktonic foraminifera over the north and west shelf of Svalbard (Ślubowska et al., 2005;

Ślubowska-Woldengen et al., 2007; Skirbekk et al., 2010; Rasmussen et al., 2014). In sediments from the central and eastern Fram Strait and southwestern Svalbard dissolution became more important, seen as reduced shell weight of planktonic foraminifera (Zamelczyk et al., 2012), poor preservation and absence of pteropods in our record (Fig. 6h), and increased fragmentation of planktonic foraminiferal shells (Rasmussen et al., 2007; Werner et al., 2016).

The cooling trend is also reflected in the benthic environment, where the Arctic-polar species *C. excavatum* appears, reaching its highest relative abundance (about 20%) around 3500 cal yrs BP (Figs 7g, 10; Table 1). The increase in percentage in *L. lobatula* indicates strong bottom current activity (Fig. 7d). Deep-sea convection and good bottom water ventilation are also indicated by the high $\delta^{13}C$ values in *C. wuellerstorfi* (Figs 5, 10). A late Holocene cooling is also evident in several records of the Nordic Seas at lower latitudes (e.g., Birks and Koç, 2002; Calvo et al., 2002; Jennings et al., 2002; Andersen et al., 2004; Kaplan and Wolfe, 2006; Justwan et al., 2008; Ólafsdóttir et al., 2010; Rasmussen and Thomsen, 2015).

The slow increase in the opportunistic species *G. uvula* during the last 3000 years, and especially after 2000 cal yrs BP, points to increased contribution of cold, productive surface waters (Fig. 6d; Table 1). The late Holocene increase of *G. uvula* is a common occurrence at the western Svalbard margin (Fig. 8a, c; Rasmussen et al., 2007; Werner et al., 2013) and western Barents Sea (Berben et al., 2014). Increase in IRD content (Fig. 4c) and in sea-ice biomarker concentration indicates a more extensive sea-ice cover and increased freshwater supply (Müller et al., 2012; Werner et al., 2013; 2016). The gradual decrease in both $\delta^{13}C$ and $\delta^{18}O$ values of *N. pachyderma* (s) in the last 3000 years observed in our record (Fig. 5) confirms a general pattern already described in the neighbouring cores MSM5/5-712-2 and MSM5/5-723-2 (Fig. 9), indicating less ventilated subsurface water with higher temperature, possibly in connection with enhanced Atlantic Water advection (Werner et al., 2013; 2016;

511 Aagaard-Sørensen et al., 2014b). These authors explain this apparent contradiction with the
512 presence of a strong pycnocline separating cold surface waters from the warm Atlantic layer
513 below and with the migration of *N. pachyderma* (s) to the deeper Atlantic layer, where
514 conditions were more favourable. Evidence for increased Atlantic Water inflow and strong
515 stratification of the upper water column has been found elsewhere in the Nordic Seas in the
516 same period (Lubinski et al., 2001; Sarnthein et al., 2003; Hald et al., 2007; Risebrobakken et
517 al., 2003; 2011; Berben et al., 2014).

518 The gradual decrease in relative abundance of *C. excavatum* and the small increase of *N.*
519 *labradorica* and *C. wuellerstorfi* (Fig. 7), together with a slight decrease in $\delta^{18}O$ values in
520 both benthic records during the last 2000 years (Fig. 5), can indicate warmer intermediate
521 waters conditions. Increased inflow of Atlantic Water and periodic stratification at the surface
522 in the last 2000 years has been described in Isfjorden, Svalbard (Rasmussen et al., 2012) and
523 in the western Barents Sea (Chistyakova et al., 2010; Dylmer et al., 2013; Groot et al., 2014).
524 However, the general conditions remained cold and unstable with episodes of reduced salinity
525 and concomitant increases in sea-ice and decreases in surface temperature (e.g., Ślubowska-
526 Woldengen et al., 2007, 2008; Risebrobakken et al., 2010; Werner et al., 2013; Berben et al.,
527 2014).

528

529 **7. Summary and conclusions**

530 Sediment core JM10-330GC from the Vestnesa Ridge (NW Svalbard margin) has been
531 investigated with regard to planktonic and benthic foraminiferal assemblages, stable isotopes,
532 and sedimentological parameters in order to reconstruct the palaeoceanographic and
533 palaeoenvironmental evolution of the eastern Fram Strait in the last 14,000 years.

The sediment record has been divided into five time-intervals reflecting different environmental and climatic conditions (Fig. 10):

1. The end of Bølling and Allerød interstadial (14,120−12,850 cal yrs BP) was relatively cold with unstable climatic conditions, influence of polar surface water, and dominance of the polar species *Neogloboquadrina pachyderma* (s). However, beneath the cold polar surface waters, chilled Atlantic-derived intermediate water was flowing at the bottom of the Vestnesa Ridge, as suggested by the high abundance of the Atlantic Water species *Cassidulina neoteretis*.
2. The Younger Dryas (12,850–11,650 cal yrs BP) was characterised in its early part by the deposition of a sandy layer associated with a meltwater event and increase in opportunistic benthic foraminiferal species (*Stainforthia loeblichi* and *Nonionella iridea*). After the meltwater event the surface water conditions were still cold with a strong influence of polar surface water, but with open water conditions that allowed seasonal, pulsed primary production. The influx of Atlantic Water at the bottom was still present, but with lower temperature and lower current velocity.
3. The early Holocene (11,650–8800 cal yrs BP) was characterised by unstable and quite cold conditions at the beginning. The shift to interglacial conditions with cold intermediate water and deep-sea convection occurred at about 11,000 cal yrs BP in the benthic environment, while in the planktonic environment the shift to warm conditions occurred later around 10,300 cal yrs BP. Climate optimum conditions were finally established around 9800 cal yrs BP.
4. The middle Holocene (8800–4100 cal yrs BP) was warmer than today with strong inflow of Atlantic water, which persisted until about 7000 cal yrs BP. The 8200 cal yrs BP climate anomaly was inconspicuous in our record. A more pronounced cool event with abrupt decrease in *Turborotalita quinqueloba* occurred between 7000 and 6200

cal yrs BP. After 6200 cal yrs BP relatively warm conditions were established again, but generally cooler than before. The persistence of warmer conditions until the end of the period suggests a delayed influence of polar water at the core site in comparison to other records in the Nordic Seas.

5. The late Holocene (4100–150 cal yrs BP) was characterised by cold climatic conditions with *N. pachyderma* (s) as the dominant species again. The polar benthic species *Cribroelphidium excavatum* appeared, indicating colder and more variable conditions. Warmer intermediate waters conditions occurred from about 2000 cal yrs BP, with periodic increases of Atlantic Water inflow.

Acknowledgements

This research is part of the Centre of Excellence: Arctic Gas hydrate, Environment and Climate (CAGE) funded by the Norwegian Research Council (grant no. 223259). Additional funding came from the European project HERMIONE of the 7th framework program environment including climate change (grant no. 226354), and from the Paleo-CIRCUS project supported by the Mohn Foundation and UiT, the Arctic University of Norway. We are grateful to the captain, crew and scientific party on board R/V *Helmer Hanssen* for help in collecting the core. We thank the staff at the Electron Microscopy Centre at Plymouth University (UK) for assistance during SEM analysis. We acknowledge the assistance of J. P. Holm for Fig. 1. Christopher W. Smart and Malcolm B. Hart are thanked for a friendly review of the manuscript. The constructive comments of two anonymous reviewers and Regional Editor Frans J. Jorissen helped to improve significantly the manuscript and are gratefully appreciated.

583 **References**

584 Aagaard, K., Foldvik, A., Hillman, S.R., 1987. The West Spitsbergen Current: disposition and
585 water mass transformation. Journal of Geophysical Research 92, 3778−3784.

586 Aagaard, K., Swift, J.H., Carmack, E.C., 1985. Thermohaline circulation in the Arctic
587 Mediterranean Seas. Journal of Geophysical Research 90, 4833–4846.

588 Aagaard-Sørensen, S., Husum, K., Hald, M., Knies, J., 2010. Paleoceanographic development
589 in the SW Barents Sea during the Late Weichselian-Early Holocene transition.
590 Quaternary Science Review 29, 3442–3456.

591 Aagaard-Sørensen, S., Husum, K., Werner, K., Spielhagen, R.F., Hald, M., Marchitto, T.M.,
592 2014a. A Late Glacial-Early Holocene multiproxy record from the eastern Fram Strait,
593 Polar North Atlantic. Marine Geology 355, 15–26.

594 Aagaard-Sørensen, S., Husum, K., Hald, M., Marchitto, T., Godtliebsen, F., 2014b. Sub sea
595 surface temperatures in the Polar North Atlantic during the Holocene: Planktic
596 foraminiferal Mg/Ca temperature reconstructions. The Holocene 24, 93–103.

597 Alve, E., 1995. Benthic foraminiferal distribution and recolonization of formerly anoxic
598 environments in Drammensfjord, southern Norway. Marine Micropalentology 25, 190–
599 203.

600 Andersen, C., Koç, N., Jennings, A., Andrews, J.T., 2004. Non uniform response of the major
601 surface currents in the Nordic seas to insolation forcing: implications for the Holocene
602 climate variability. Paleoceanography 19, PA2003, doi:10.1029/2002PA000873.

603 Bauch, H.A., Erlenkeuser, H., Spielhagen, R.F., Struck, U., Matthiessen, J., Thiede, J.,
604 Heinemeier, J., 2001. A multiproxy reconstruction of the evolution of deep and surface
605 waters in the subarctic Nordic seas over the last 30,000 yr. Quaternary Science Reviews
606 20, 659–678, http://dx.doi.org/10.1016/S0277-3791(00)00098-6.

607 Bé, A.W.H., Tolderlund, D.S., 1971. Distribution and ecology of living planktonic
608 foraminifera in surface waters of the Atlantic and Indian Oceans. In: Funnell, B.M.,
609 Riedel, W.R. (Eds.), The Micropaleontology of the Oceans. Cambridge University
610 Press, 105−149.

611 Belanger, B.E., Streeter, S.S., 1980. Distribution and ecology of benthic foramnifera in the
612 Norwegian-Greenland Sea. Marine Micropaleontology 5, 401−428.

613 Berben, S.M.P., Husum, K., Cabedo-Sanz, P., Belt, S.T., 2014. Holocene sub-centennial
614 evolution of Atlantic water inflow and sea ice distribution in the western Barents Sea.
615 Climate of the Past 10, 181−198, doi:10.5194/cp-10-181-2014.

616 Bergami, C., Capotondi, L., Langone, L., Giglio, F., Ravaioli, M., 2009. Distribution of living
617 planktonic foraminifera in the Ross Sea and the Pacific sector of the Southern Ocean
618 (Antarctica). Marine Micropaleontolology 73, 37–48.

619 Berger, W.H., 1970. Planktonic foraminifera: Selective solution and the lysocline. Marine
620 Geology 8 (2), 111−138.

621 Birgel, D., Hass, H.C., 2004. Oceanic and atmospheric variations during the last deglaciation
622 in the Fram Strait (Arctic Ocean): a coupled high-resolution organic-geochemical and
623 sedimentological study. Quaternary Science Reviews 23 (1–2), 29–47,
624 http://dx.doi.org/10.1016/j.quascirev.2003.10.001.

625 Birks, C.J.A., Koç, N., 2002. A high-resolution diatom record of late-Quaternary sea- surface
626 temperatures and oceanographic conditions from the eastern Norwegian Sea. Boreas 31,
627 323–344.

628 Boltovskoy, E., Boltovskoy, D., Correa, N., Brandini, F., 1996. Planktic foraminifera from the
629 southwestern Atlantic (30°–60°S): species-specific patterns in the upper 50 m. Marine
630 Micropaleontology 28, 53–72.

631 Bünz, S., Polyanov, S., Vadakkepuliyambatta, S., Consolaro, C., Mienert, J., 2012. Active gas
632 venting trough hydrate-bearing sediments on the Vestnesa Ridge, offshore W-Svalbard.
633 Marine Geolology 332-334, 189−197.

634 Calvo, E., Grimalt, J., Jansen, E., 2002. High resolution U^{K}_{37} sea surface temperature
635 reconstruction in the Norwegian Sea during the Holocene. Quaternary Science Reviews
636 21, 1385–1394.

637 Carstens, J., Hebbeln, D., Wefer, G., 1997. Distribution of planktic foraminifera at the ice
638 margin in the Arctic (Fram Strait). Marine Micropaleontology 29, 257−269.

639 Cherns, L., Wright, V.P., 2009. Quantifying the impact of early diagenetic aragonite
640 dissolution on the fossil record. Palaios 24, 756−771.

641 Chistyakova, N.O., Ivanova, E.V., Risebrobakken, B., Ovsepyan, E.A., Ovsepyan, Y.S., 2010.
642 Reconstruction of the postglacial environments in the southwestern Barents Sea based
643 on foraminiferal assemblages. Oceanology 50, 573–581.

644 Consolaro, C., Rasmussen, T.L., Panieri, G., Mienert, J., Bunz, S., Sztybor, K., 2015. Carbon
645 isotope ($\delta^{13}C$) excursions suggest times of major methane release during the last 14 kyr
646 in Fram Strait, the deep-water gateway to the Arctic. Climate of the Past 11, 669–685.

647 Darling, K.F., Kucera, M., Kroon, D., Wade, C.M., 2006. A resolution for the coiling
648 direction paradox in *Neogloboquadrina pachyderma*. Paleoceanography 21, PA2011,
649 doi:10-1029/2005PA001189.

650 Duffield, C.J., Hess, S., Norling, K., Alve, E., 2015. The response of *Nonionella iridea* and
651 other benthic foraminifera to 'fresh' organic matter enrichment and physical
652 disturbance. Marine Micropaleontolology 120, 20–30.

653 Duplessy, J.-C., Moyes, J., Pujol, C., 1980. Deep water formation in the North Atlantic Ocean
654 during the last ice age. Nature 286, 479–482.

655 Dylmer, C.V., Giraudeau, J., Eynaud, F., Husum, K., De Vernal, A., 2013. Northward
656 advection of Atlantic water in the eastern Nordic Seas over the last 3000 yr: A coccolith
657 investigation of volume transport and surface water changes. Climate of the Past 9,
658 1505–1518, doi:10.5194/cp-9-1505–2013.

659 Ebbesen, H., Hald, M., Eplet, T.H., 2007. Late glacial and early Holocene climatic
660 oscillations on the western Svalbard margin, European Arctic. Quaternary Science
661 Review 26, 1999−2011.

662 Ehrmann, W.U., Thiede, J., 1985. History of Mesozoic and Cenozoic sediment flux to the
663 North Atlantic Ocean. Contribution to Sedimentology 15, 1−109.

664 Espitalié, J., Laporte, J.L., Madec, M., Marquis, F., Leplat, P., Paulet, J., Boutefeu, A., 1977.
665 Méthode rapide de characterization des roches-mere, de leur potential petrolier et de
666 leur degree d'évolution. Revue de l'Institute Francais du Petrole 32, 23−42.

667 Fairbanks, R.G., 1989. A 17,000-year glacio-eustatic sea level record: influence of glacial
668 melting rates on the Younger Dryas event and deep-ocean circulation. Nature 342,
669 637−742.

670 Gooday, A.J., 1988. A response by benthic foraminifera to the deposition of phytodetritus in
671 the deep sea. Nature 332, 3–70.

672 Gooday, A.J., Hughes, J.A., 2002. Foraminifera associated with phytodetritus deposits at a
673 bathyal site in the northern Rockall Trough (NE Atlantic): seasonal contrasts and a
674 comparison of stained and dead assemblages. Marine Micropaleontology 46, 83−110.

675 Gradinger, R.R., Baumann, M.E.M., 1991. Distribution of phytoplankton communities in
676 relation to the large-scale hydrographical regime in the Fram Strait. Marine Biology
677 111, 311–321.

678 Groot, D.E., Aagaard-Sørensen, S., Husum, K., 2014. Reconstruction of Atlantic water
679 variability during the Holocene in the western Barents Sea. Climate of the Past 10, 51–
680 62, doi:10.5194/cp-10-51-2014.

681 Haake, F.-W., Pflaumann, U.W.E., 1989. Late Pleistocene foraminiferal stratigraphy on the
682 Vøring Plateau, Norwegian Sea. Boreas 18, 343–356.

683 Hald, M., Steinsund, P.I., 1992. Distribution of surface sediment benthic foraminifera in the
684 southwestern Barents Sea. Journal of Foraminiferal Research 22, 347−362.

685 Hald, M., Korsun, S., 1997. Distribution of modern benthic foraminifera from fjords of
686 Svalbard, European Arctic. Journal of Foraminiferal Research 27, 101−122.

687 Hald, M., Ebbesen, H., Forwick, M., Godtliebsen, F., Khomenko, L., Korsun, S., Olsen, L.R.,
688 Vorren, T.O., 2004. Holocene paleoceanography and glacial history of the west
689 Spitsbergen area, Euro-Arctic margin. Quaternary Science Review 23, 2075−2088.

690 Hald, M., Kolstad, V., Polyak, L., Forman, S. L., Herlihy, F. A., Ivanov, G., Nescheretov, A.,
691 1999. Late-glacial and Holocene paleoceanography and sedimentary environments in
692 the St. Anna Trough, Eurasian Arctic Ocean margin. Palaeogeography,
693 Palaeoclimatology, Palaeoecology 146, 229–249.

694 Hald, M., Andersson, C., Ebbesen, H., Jansen, E., Klitegaard-Kristensen, D., Risebrobakken,
695 B., Salomonsen, G. R., Sejrup, H. P., Sarnthein, M., Telford, R., 2007. Variations in
696 temperature and extent of Atlantic water in the northern North Atlantic during the
697 Holocene, Quaternary Science Review 26, 3423–3440.

698 Hirche, H.-J., Baumann, M.E.M., Kattner, G., Gradinger, R., 1991. Plankton distribution and
699 the impact of copepod grazing on primary production in Fram Strait, Greenland Sea.
700 Journal of Marine Systems 2, 477–494.

701 Hopkins, T.S., 1991. The GIN Sea: A synthesis of its physical oceanography and literature
702 review, 1972–1985. Earth Science Review 30, 175–318.

703 Hustoft, S., Bunz, S., Mienert, J., Chand, S., 2009. Gas hydrate reservoir and active methane-
704 venting province in sediments on <20 Ma young oceanic crust in the Fram Strait,
705 offshore NW-Svalbard. Earth and Planetary Science Letters 284, 12−24.

706 Jansen, E., Sejrup, H.P., Fjaeran, T., Hald, M., Holtedahl, H., Skarbø O., 1983. Late
707 Weichselian paleoceanography of the southeastern Norwegian Sea. Norsk Geologisk
708 Tidsskrift 63, 117–146.

709 Jennings, A.E., Weiner, N.J., 1996. Environmental change in eastern Greenland during the
710 last 1300 years: evidence from foraminifera and lithofacies in Nansen Fjord, 68 degree
711 N. The Holocene 6, 179−191.

712 Jennings, A.E., Hald, M., Smith, M., Andrews, J.T., 2006. Freshwater forcing from the
713 Greenland Ice Sheet during the Younger Dryas: evidence from southeastern Greenland
714 shelf cores. Quaternary Science Review 25, 282−298.

715 Jennings, A.E., Knudsen, K.L., Hald, M., Hansen, C.V., Andrews, J.T., 2002. A mid-
716 Holocene shift in Arctic sea-ice variability on the East Greenland Shelf. The Holocene
717 12, 49–58.

718 Jessen, S.P., Rasmussen, T.L., Nielsen, T., Solheim, A., 2010. A new Late Weichselian and
719 Holocene marine chronology for the western Svalbard slope 30,000-0 cal years BP.
720 Quaternary Science Reviews 29, 1301−1312.

721 Jorissen, F.J., Fontanier, C., Thomas, E., 2007. Paleoceanographical proxies based on deep-
722 sea benthic foraminiferal assemblage characteristics. In: Hillaire-Marcel, E., de Vernal,
723 C. (Eds), Proxies in Late Cenozoic Paleoceanography, Pt. 2: Biological Tracers and
724 Biomarkers, Developments in Marine Geology 1, 263−326.

725 Judd, A.G., Hovland, M., 2007. Seabed Fluid Flow: the Impact on Geology, Biology, and the
726 Marine Environment. Cambridge University, Cambridge, 475 pp.

727 Justwan, A., Koç, N., Jennings, A.E., 2008. Evolution of the Irminger and East Icelandic
728 Current systems through the Holocene, revealed by diatom-based sea surface
729 temperature reconstructions. Quaternary Science Reviews 27, 1571–1582.

730 Kaplan, M.R., Wolfe, A.P., 2006. Spatial and temporal variability of Holocene temperature in
731 the North Atlantic region. Quaternary Research 65, 223–231.

732 Klitgaard-Kristensen, D., Rasmussen, T.L., Koç, N., 2013. Palaeoceanographic changes in the
733 northern Barents Sea during the last 16 000 years – new constraints on the last
734 deglaciation of the Svalbard-Barents Sea Ice Sheet. Boreas 42, 798−813.

735 Knies, J., Vogt, C., Stein, R., 1999. Growth and decay patterns of the Svalbard/Barents Sea-
736 ice sheet and palaeoceanographic evolution during Saalian and Weichselian glaciations.
737 Geo Marine Letters 18, 195–202.

738 Knies, J., Müller, C., Nowaczyk, N., Stein, R., 2000. A multi-proxy approach to reconstruct
739 the environmental changes along the Eurasian continental margin over the last 160000
740 years. Marine Geology 163, 317–344.

741 Knudsen, K.L., 1998. Foraminifer I Kvartær stratigrafi: Laboratorie og fremstillingsteknik
742 samt udvalgte eksempler. Geologisk Tidsskrift 3, 1–25.

743 Knudsen, K.L., Jiang, H., Jansen, E., Eiriksson, J., Heinemeier, J., Seidenkrantz, M.S., 2004.
744 Environmental changes off North Iceland during the deglaciation and the Holocene:
745 foraminifera, diatoms and stable isotopes. Marine Micropaleontology 50, 273–305.

746 Koç, N., Klitgaard-Kristensen, D., Hasle, K., Forsberger, C.F., Solheim, A., 2002. Late
747 glacial palaeoceanography of Hinlopen Strait, northern Svalbard. Polar Research 21,
748 307−314.

749 Korsun, S., Hald, M., 1998. Modern benthic foraminifera off Novaya Zemlya tidewater
750 glaciers, Russian Arctic. Arctic and Alpine Research 30, 61−77.

751 Korsun, S., Hald, M., 2000. Seasonal dynamics of benthic foraminifera in a glacially fed fjord
752 of Svalbard, European Arctic. Journal of Foraminiferal Research 30, 251–271.

753 Landvik, J.Y., Bondevik, S., Elverhøi, A., Fjeldskaar, W., Mangerud, J., Salvigsen, O.,
754 Siegert, M.J., Svendsen, J.-I., Vorren, T.O., 1998. The last glacial maximum of
755 Svalbard and the Barents Sea: ice sheet extent and configuration. Quaternary Science
756 Reviews 17, 43–77.

Loeblich, A.R., Tappan, H., 1987. Foraminiferal Genera and their Classification. Van Nostrand Reinhold, New York, 212 pp.

Lubinski, D.J., Korsun, S., Polyak, L., Forman, S.L., Lehman, S.J., Herlihy, F., Miller, G.H., 1996. The last deglaciation of the Franz Victoria Trough, northern Barents Sea. Boreas 25, 89–100.

Lubinski, D.J., Polyak, L., Forman, S.L., 2001. Freshwater and Atlantic water inflows to the deep northern Barents and Kara seas since ca. 13 14C ka: foraminifera and stable isotopes. Quaternary Science Reviews 20, 1851–1879.

Mackensen, A., Hald, M., 1988. *Cassidulina teretis* Tappan and *C. laevigata* d'Orbigny: their modern and Late Quaternary distribution in northern seas. Journal of Foraminiferal Research 18, 16–24.

Mackensen, A., Sejrup, H.-P., Jansen, E., 1985. The distribution of living benthic foraminifera on the continental slope and rise off southwest Norway. Marine Micropaleontology 9, 275–306.

Mangerud, J., Bolstad, M., Elgersma, A., Helliksen, D., Landvik, J.Y., Lønne, L., Lycke, A.K., Salvigsen, O., Sandahl, T., Svendsen, J.I., 1992. The last glacial maximum on Spitsbergen, Svalbard. Quaternary Research 38, 1–31.

Müller, J., Stein, R., 2014. High resolution record of late glacial and deglacial sea ice changes in Fram Strait corroborates ice-ocean interactions during abrupt climate shifts. Earth and Planetary Science Letters 403, 446–455.

Müller, J., Massé, G., Stein, R., Belt, S.T., 2009. Variability of sea-ice conditions in the Fram Strait over the past 30,000 years. Nature Geoscience 2, 772–776.

Müller, J., Werner, K., Stein, R., Fahal, K., Moros, M., Jansen, E., 2012. Holocene cooling culminates in sea ice oscillations in Fram Strait. Quaternary Science Review 47, 1–14.

Murgese, D.S., de Decker, P., 2005. The distribution of deep-sea benthic foraminifera in core tops from the eastern Indian Ocean. Marine Micropaleontology 56, 25–49.

Murray, J., 2006. Ecology and applications of benthic foraminifera. Cambridge University Press, Cambridge, 422 pp.

Nørgaard-Pedersen, N., Spielhagen, R.F., Erlenkeuser, H., Grootes, P.M., Heinemeier, J., Knies, J., 2003. Arctic Ocean during the last glacial maximum: Atlantic and polar

787 domains of surface water mass distribution and ice cover. Paleoceanography 18, 1063,
788 doi:10.1029/2002PA000781.

789 NSIDC (National Snow, Ice Data Center), 2016. Brightness temperature and ice
790 concentrations grids for the polar regions. User's guide. NSIDC Distributed Active
791 Archive Center, Boulder, Colorado.

792 Ólafsdóttir, S., Jennings, A.E., Geirsdóttir, A., Andrews, J., Miller, G.H., 2010. Holocene
793 variability of the North Atlantic Irminger current on the south- and northwest shelf of
794 Iceland. Marine Micropaleontology 77, 101–118.

795 Polyak, L., Solheim, A., 1994. Late-and postglacial environments in the northern Barents Sea
796 west of Franz Josef Land. Polar Research 13, 197−207.

797 Polyak, L., Korsun, S., Febo, L.A., Stanovoy, V., Khusid, T., Hald, M., Paulsen, B.E.,
798 Lubinski, D.J., 2002. Benthic foraminiferal assemblages from the southern Kara Sea, a
799 river-influenced arctic marine environment. Journal of Foraminiferal Research 32,
800 252−273.

801 Rasmussen, T.L., Thomsen, E., 2015. Palaeoceanographic development in Storfjorden,
802 Svalbard, during the deglaciation and Holocene: evidence from benthic foraminiferal
803 records. Boreas 44, 24−44. DOI: 10.1111/bor.12098.

804 Rasmussen, T.L., Balbon, E., Thomsen, E., Labeyrie, L., Van Weering, T.C.E., 1999. Climate
805 records and changes in deep outflow from the Norwegian Sea ~150–55 ka. Terra Nova
806 11, 61–66.

807 Rasmussen, T.L., Thomsen, E., Ślubowska, M.A., Jessen, S., Solheim, A., Koç, N., 2007.
808 Paleoceanographic evolution of the SW Svalbard margin (76°N) since 20,000 ^{14}C yr
809 BP. Quaternary Research 67, 100−114.

810 Rasmussen, T.L., Forwick, M., Mackensen, A., 2012. Reconstruction of inflow of Atlantic
811 Water to Isfjorden, Svalbard during the Holocene: correlation to climate and
812 seasonality. Marine Micropaleontology 94-95, 80–90.

813 Rasmussen, T.L., Thomsen, E., Skirbekk, K., Ślubowska-Woldengen, M.A., Klitgaard-
814 Kristensen, D., Koç, N., 2014. Spatial and temporal distribution of Holocene
815 temperature maxima on the northern Nordic seas: interplay of Atlantic-, Arctic- and
816 polar water masses. Quaternary Research 92, 280−291.

817 Rasmussen, T.L., Thomsen, E., 2017. Ecology of deep-sea benthic foraminifera in the North
818 Atlantic during the last glaciation: food or temperature control. Palaeogeography,
819 Palaeoclimatology, Palaeoecology 472, 15–32.

820 Risebrobakken, B., Moros, M., Ivanova, E.V., Chistyakova, N., Rosenberg, R., 2010. Climate
821 and oceanographic variability in the SW Barents Sea during the Holocene. The
822 Holocene 20, 609–621.

823 Risebrobakken, B., Dokken, T., Smedsrud, L.H., Andersson, C., Jansen, E., Moros, M.,
824 Ivanova, E.V., 2011. Early Holocene temperature variability in the Nordic Seas: The
825 role of oceanic heat advection versus changes in orbital forcing. Paleoceanography 26,
826 PA4206, doi:10.1029/2011PA002117.

827 Rytter, F., Knudsen, K.L., Seidenkrantz, M.S., Eiriksson, J., 2002. Modern distribution of
828 benthic foraminifera on the North Icelandic shelf and slope. The Journal of
829 Foraminiferal Research 32, 217–244.

830 Sarnthein, M., Van Kreveld, S., Erlenkeuser, H., Grootes, P.M., Kucera, M., Pflaumann, U.,
831 Schulz, M., 2003. Centennial-to-millenial-scale periodicities of Holocene climate and
832 sediment injections off the western Barents shelf, 75°N. Boreas 32, 447−461.

833 Scott D.B, Vilks, G., 1991. Benthonic foraminifera in the surface sediments of the deep-sea
834 Arctic Ocean. Journal of Foraminiferal Research 21, 20−38.

835 Sejrup, H.-P., Fjæran, T., Hald, M., Beck, L., Hagen, J., Miljeteig, I., Morvik, I., Norvik, O.,
836 1981. Benthonic foraminifera in surface samples from the Norwegian continental
837 margin between 62°N and 65°N. Journal of Foraminiferal Research 11, 277−295.

838 Sejrup, H., Birks, H., Klitgaard-Kristensen, D., Madsen, H., 2004. Benthonic foraminiferal
839 distributions and quantitative transfer functions for the northwest European continental
840 margin. Marine Micropaleontology 53, 197–226.

841 Simstich, J., Sarnthein, M., Erlenkeuser, H., 2003. Paired $\delta^{18}O$ signals of *Neogloboquadrina*
842 *pachyderma* (s) and *Turborotalita quinqueloba* show thermal stratification structure in
843 Nordic Seas. Marine Micropaleontology 48, 107−125.

844 Skirbekk, K., Klitgaard-Kristensen, D., Rasmussen, T.L., Koç, N., Forwick, M., 2010.
845 Holocene climate variations at the entrance to a warm Arctic fjord: evidence from

Kongsfjorden trough, Svalbard. Geological Society, London, Special Publications 344, 289–304.

Ślubowska, M.A., Koç, N., Rasmussen, T.L., Klitgaard-Kristensen, D., 2005. Changes in the flow of Atlantic water into the Arctic Ocean since the last deglaciation: Evidence from the northern Svalbard continental margin, 80°N. Paleoceanography 20, PA4014, doi: 10.1029/2005PA001141.

Ślubowska-Woldengen M., Rasmussen, T.L., Koç, N., Klitgaard-Kristensen, D., Nilsen, F., Solheim, A., 2007. Advection of Atlantic Water to the western and northern Svalbard shelf since 17,500 cal yr BP. Quaternary Science Reviews 26, 463−478.

Ślubowska-Woldengen, M., Koç, N., Rasmussen, T.L., Klitgaard-Kristensen, D., Hald, M., Jennings, A.E., 2008. Time-slice reconstructions of ocean circulation changes on the continental shelf in the Nordic and Barents Seas during the last 16 000 cal yr B.P. Quaternary Science Reviews 27, 1476–1492.

Smart, C.W., King, S.C., Gooday, A.J., Murray, J.W., Thomas, E., 1994. A benthic foraminiferal proxy of pulsed organic matter paleofluxes. Marine Micropaleontology 23, 89−99.

Smith Jr.W.O., Baumann, M.E.M., Wilson, D.L., Aletsee, L., 1987. Phytoplankton biomass and productivity in the marginal ice zone of the Fram Strait during summer 1984. Journal of Geophysical Research 92, 6777–6786.

Stabell, B., 1986. A diatom maximum horizon in upper Quaternary deposits. Geologishes Rundschau 75, 175–184.

Thomas, E., Booth, L., Maslin, M., Shackleton, N.J., 1995. Northeastern Atlantic benthic foraminifera during the last 45,000 years: changes in productivity seen from the bottom up. Paleoceanography 10, 545–562.

Vinje, T.E., 1977. Sea ice conditions in the European sector of the marginal seas of the Arctic 1966–75. Norwegian Polar Institut 1975, 163–174.

Vogt, P.R., Crane, K., Sundvor, E., Max, M.D., Pfirman, S.L., 1994. Methane-generated (?) pockmarks on young, thickly sedimented oceanic crust in the Arctic: Vestnesa ridge, Fram Strait. Geology 22, 255−258.

Volkmann, R., 2000. Planktic foraminifers in the outer Laptev Sea and the Fram Strait: Modern distribution and ecology. Journal of Foraminiferal Research 30, 157−176.

Vorren, T.O., Kristoffersen, Y., 1986. Late Quaternary glaciation in the southwestern Barents Sea. Boreas 15, 51−60.

Werner, K., Spielhagen, R.F., Bauch, D., Hass, H.C., Kandiano, E., 2013. Atlantic Water advection versus sea-ice advances in the eastern Fram Strait during the last 9 ka: Multiproxy evidence for a two-phase Holocene. Paleoceanography 28, 283–295, doi:10.1002/palo.20028.

Werner, K., Müller, J., Husum, K., Spielhagen, R.F., Kandiano, E.S., Polyak, L., 2016. Holocene sea subsurface and surface water masses in the Fram Strait – Comparisons of temperature and sea-ice reconstructions. Quaternary Science Reviews 147, 194–209.

Wollenburg, J.E., Mackensen, A., 1998. Living benthic foraminifers from the central Arctic Ocean: faunal composition, standing stock and diversity. Marine Micropaleontology 34, 153−185.

Wollenburg, J.E., Knies, J., Mackensen, A., 2004. High-resolution paleoproductivity fluctuations during the last 24 kyr as indicated by benthic foraminifera in the marginal Arctic Ocean. Palaeogeography, Palaeoclimate, Palaeoecology 204, 209−238.

Zamelczyk, K., Rasmussen, T.L., Husum, K., Haflidason, H., de Vernal, A., Ravna, E.K., Hald, M., Hillaire-Marcel, C., 2012. Paleoceanographic changes and calcium carbonate dissolution in the central Fram Strait during the last 20 ka yr. Quaternary Research 78, 405–416. http://dx.doi.org/10.1016/j.yqres.2012.07.006.

Figure captions

Fig. 1. Bathymetric map showing major surface currents in the Nordic Seas and Barents Sea, and the core location (black circle). Black dashed line: modern position of the Polar Front. Black line: modern position of the Arctic Front. Abbreviations: NAC: North Atlantic Current; WSC: West Spitsbergen Current; ESC: East Spitsbergen Current; EGC: East Greenland Current; DS: Denmark Strait. Figure is modified after Consolaro et al. (2015).

Fig. 2. A) Bathymetric map of the W-Svalbard margin and eastern Fram Strait. Abbreviations: MFZ: Molloy Fracture Zone; MD: Molloy Deep; MR: Molloy Ridge; SFZ: Spitsbergen Fracture Zone; YP: Yermak Plateau. B) Overview swath bathymetry map of the Vestnesa Ridge. Black circles indicate the location of the studied core JM10-330GC and CTD. White circles indicate location of other cores discussed in the paper: MSM5/5-712-2 (Werner et al., 2013; Aagaard-Sørensen et al., 2014a,b), MSM5/5-723-2 (Werner et al., 2016); core 1 (JM03-373PC2: Rasmussen et al., 2007; Jessen et al., 2010), and core 2 (MD99-2304: Ebbsen et al., 2007). Figures are modified after Consolaro et al. (2015).

Fig. 3. Conductivity-temperature-depth (CTD) data of temperature and salinity from the core site taken on June 27, 2010. Abbreviations: AW: Atlantic Water; GSIW: Greenland Sea Intermediate Water.

Fig. 4. Sedimentological and geochemical data plotted versus cal kyrs BP. (a) Calculated sediment accumulation rate. (b) Grain size distribution in %. (c) Number of ice-rafted debris (IRD) >1 mm (black) and concentration of IRD >100 μm per gram dry weight sediment (red line). (d) Concentration of diatoms (magenta), siliceous remains (radiolarian and sponge spicules; blue), and pyritized burrows (brown line) >100 μm per gram dry weight sediment. (e) CaCO3 wt% (grey) and TOC wt% (black line). (f) Stratigraphy obtained for JM10-330GC with chronological subdivisions (black lines). White diamonds on the *y* axis indicate radiocarbon dated levels. Abbreviations: B-A: Bølling-Allerød; YD: Younger Dryas; sl: sandy layer; E-H: early Holocene.

Fig. 5. Isotopic records plotted versus cal kyrs BP. Left: $\delta^{18}O_{IVC}$ (ice volume corrected) record of *Cassidulina neoteretis* (red line), *Cibicides wuellerstorfi* (green line) and *N. pachyderma* (s) (blue line). Right: $\delta^{13}C$ record of *C. neoteretis* (red line), *C. wuellerstorfi* (green line) and *N. pachyderma* (s) (blue line). Dotted vertical lines mark average stable isotope values of species. White diamonds on the *y* axis indicate radiocarbon dated levels. Shaded horizontal bars indicate carbon isotope excursions CIE I and CIE II (Consolaro et al., 2015). Abbreviations: IVC: ice volume corrected; B-A: Bølling-Allerød; YD: Younger Dryas; sl: sandy layer.

936

937

938 Fig. 6. Relative abundance (%; grey) and flux (black line) of planktonic foraminifera plotted
939 versus cal kyrs BP; (a) *Neogloboquadrina pachyderma* (s); (b) *Turborotalita quinqueloba*; (c)
940 *N. pachyderma* (d); (d) *Globigerinita uvula*; (e) *Globigerinita glutinata*; (f) *Globigerina*
941 *bulloides*; (g) Concentration of planktonic foraminifera per gram dry weight sediment (grey)
942 and planktonic foraminifera flux (black line); (h) Presence of pteropods. White diamonds on
943 the *y* axis indicate radiocarbon dated levels.

944

945 Fig. 7. Relative abundance (%; grey) and flux (black line) of benthic foraminifera plotted
946 versus cal kyrs BP. (a) *Cassidulina neoteretis;* (b) *C. reniforme;* (c) *Melonis barleeanus;* (d)
947 *Lobatula lobatula*; (e) *Cibicides wuellerstorfi*; (f) *Epistominella arctica*; (g) *Cribroelphidium*
948 *excavatum*; (h) *Oridorsalis umbonatus*; (i) *Ioanella tumidula*; (j) *Stainforthia loeblichi*; (k)
949 *Nonionella iridea*; (l) *Nonionellina labradorica*; (m) Miliolids; (n) Agglutinated; (o)
950 Concentration of benthic foraminifera per gram dry weight sediment (grey) and benthic
951 foraminifera flux (black line). White diamonds on the *y* axis indicate radiocarbon dated levels.

952

953 Fig. 8. Comparison of planktonic foraminiferal records of JM10-330GC with other records
954 from the western Svalbard margin. (a) Core JM03-373PC (b) core MD99-2304 (c) core
955 MSM5/5-712-2 (d) core JM10-330GC and (e) core MSM5/5-712-2.

956

957 Fig. 9. Comparison of *C. wuellerstorfi* and *N. pachyderma* (s) isotopic records of JM10-
958 330GC with other records from the western Svalbard margin. (a–c) $\delta^{18}O_{IVC}$ records of *C.*
959 *wuellerstorfi*; (d–h) $\delta^{18}O_{IVC}$ records of *N. pachyderma* (s); (i–l) $\delta^{13}C$ records of *N.*
960 *pachyderma* (s); (m–o) $\delta^{13}C$ records of *C. wuellerstorfi*. Data for a, m (Werner et al., 2013);
961 b, g, k, n (this study); c, h, l, o (Werner et al., 2016); d (Rasmussen et al., 2007); e, j (Ebbesen
962 et al., 2007); f, j (Werner et al., 2013; Aagaard-Sørensen et al., 2014a).

963

964 Fig. 10. Schematic overview with the main parameters of core JM10-330GC plotted versus
965 cal kyrs BP, and their interpretation. (a) $\delta^{18}O_{IVC}$ record of *Cibicides wuellerstorfi* (green) and

966 *N. pachyderma* (s) (blue); Relative abundance (%) of: (b) *T. quinqueloba* (magenta) and *N.*
967 *pachyderma* (s) (blue, inverse scale); (c) *C. neoteretis* (red) and *C. reniforme* (light blue,
968 inverse scale); (d) *C. wuellerstorfi* (dark green) and *C. excavatum* (deep purple, inverse scale);
969 (e) $\delta^{13}C$ record of *Cibicides wuellerstorfi* (green) and *N. pachyderma* (s) (blue); (f)
970 Concentration of planktonic (green) and benthic (orange) foraminifera per gram dry weight
971 sediment; (g) Interpretation of the environmental conditions at the surface (S) and at the
972 bottom (B). Blue star: omitted data because the isotopic signal in the B-A is disturbed by CIE
973 I. Green star: omitted data because the number of planktonic foraminifera in the sandy layer is
974 much higher. Abbreviations: AW: Atlantic Water; Convection: deep-sea convection.

975

976 Fig. 11. Scanning electron microscope images of important benthic foraminiferal species from
977 core JM10-330GC (scale bar = 100 μm). 1, 2. *Adercotryma glomerata* 0–1 cm. 3, 4.
978 *Ammoglobigerina globigeriniformis* 0–1 cm. 5, 6. *Trochammina nana* 300–3001 cm. 7, 8.
979 *Veleroninoides wiesneri* 5–6 cm. 9. *Lagenammina micacea* 0–1 cm. 10. *Textularia earlandi*
980 0–1 cm. 11, 12. *Bolivinella pseudopunctata* 300–301 cm. 13. *Stainforthia feylingi* 0–1 cm. 14.
981 *Stainforthia loeblichi* 355–356 cm. 15, 16. *Cassidulina neoteretis* 0–1 cm. 17, 18. *Cassidulina*
982 *reniforme* 0–1 cm. 19. *Epistominella arctica* 0–1 cm. 20. *Eilohedra vitrea* 300–3001 cm.

983

984 Fig. 12. Scanning electron microscope images of important benthic foraminiferal species from
985 core JM10-330GC (scale bar = 100 μm). 21, 22. *Eilohedra nipponica* 0–1 cm. 23, 24.
986 *Lobatula lobatula* 0–1 cm. 25, 26. *Cibicides wuellerstorfi* 0–1 cm. 27. *Ioanella tumidula* 0–1
987 cm. 28. *Ioanella tumidula* 15–16 cm. 29. *Oridorsalis umbonatus* 0–1 cm. 30. *Pullenia*
988 *osloensis* 355–356 cm. 31, 32. *Pullenia bulloides* 0–1 cm. 33, 34. *Melonis barleeanus* 0–1
989 cm. 35, 36. *Cribroelphidium excavatum* 0–1 cm. 37. *Nonionellina labradorica* 5–6 cm. 38,
990 39. *Nonionella stella* 355–356 cm. 40, 41. *Nonionella iridea* 5–6 cm. Scale bar is 100 μm.

991

992 **Taxonomic Appendix**

993 **Planktonic foraminifera**

994 *Globigerina bulloides* d'Orbigny, 1826

995 *Globigerinita glutinata* (Egger, 1893) = *Globigerina glutinata* Egger, 1895

Globigerinita uvula (Ehrenberg, 1861) = *Globigerina bradyi* Wiesner, 1931

Neogloboquadrina pachyderma (Ehrenberg, 1861) = *Planulina pachyderma* Ehrenberg, 1854

Turborotalita quinqueloba (Natland, 1938) = *Globigerina quinqueloba* Natland, 1938

Benthic foraminifera

Adercotryma glomerata (Brady, 1878) = *Lituola glomerata* Brady, 1878

Ammoglobigerina globigeriniformis (Parker and Jones, 1865) = *Lituola nautiloides* var. *globigeriniformis* Parker and Jones, 1865

Astrononion gallowayi Loeblich and Tappan, 1953

Bolivinella pseudopunctata (Höglund, 1947) = *Bolivina pseudopunctata* Höglund, 1947

Bucella frigida (Cushman, 1921) = *Pulvinulina frigida* Cushman, 1921

Cassidulina laevigata d'Orbigny, 1826

Cassidulina neoteretis Seidenkrantz, 1995

Cassidulina reniforme Nørvang, 1945

Cibicides sp. de Montfort, 1808

Cibicides wuellerstorfi (Schwager, 1866) = *Anomalina wuellerstorfi* Schwager, 1866

Cribroelphidium excavatum (Terquem, 1875) = *Polystomella excavata* Terquem, 1875

Cribrostomoides subglobosus (Cushman, 1910) = *Haplophragmoides subglobosum* Cushman, 1910

Cornuspira involvens (Reuss, 1850) = *Operculina involvens* Reuss, 1850

Dentalina sp. d'Orbigny, 1826

Discorbis sp. Lamarck, 1804

Earlandammina inconspicua Earland, 1934

Eilohedra nipponica Kuwano, 1962

Eilohedra vitrea (Parker, 1953) = *Epistominella vitrea* Parker, 1953

Elphidium sp. de Montfort, 1808

Epistominella arctica Green, 1959 (with this name we include all the intergradational series of *Stetsonia horvathi* Green, 1959 and *E. arctica*, according to Scott and Vilks, 1991).

Epistominella exigua (Brady, 1884) = *Pulvinalina exigua* Brady, 1884

Evolvocassidulina bradyi (Norman, 1881) = *Cassidulina bradyi* Norman, 1881

Fissurina sp. Reuss, 1850

Fursenkoina sp. Loeblich and Tappan, 1961

Gavelinopsis praegeri (Heron-Allen and Earland, 1913) = *Discorbina praegeri* Heron-Allen and Earland, 1913

Glandulina d'Orbigny, 1839

Globobulimina Cushman, 1927

Guttulina sp. d'Orbigny, 1839

Gyroidina lamarckiana (d'Orbigny, 1839) = *Rotalina lamarckiana* d'Orbigny, 1839

Haynesina germanica (Ehrenberg, 1840) = *Nonionina germanica* Ehrenberg, 1840

Haynesina orbiculare (Brady, 1881) = *Nonion orbiculare* Brady, 1881

Ioanella tumidula (Brady, 1884) = *Truncatulina tumidula* Brady, 1884

Islandiella helenae Feyling-Hanssen and Buzas, 1976

Islandiella norcrossi (Cushman, 1933) = *Cassidulina norcrossi* Cushman, 1933

Lagena sp. Walker and Boys, 1798

Lagena striata (d'Orbigny, 1839) = *Oolina striata* d'Orbigny, 1839

Lagenammina micacea (Cushman, 1918) = *Proteonina micacea* Cushman, 1918

Lenticulina sp. Lamarck, 1804

Marginulina sp. d'Orbigny, 1826

Melonis barleeanus (Williamson, 1858) = *Nionionina barleeana* Williamson, 1858

Miliolinella sp. Wiesner, 1931

Nodosaria sp. Lamarck, 1816

Nonionella sp. Rhumbler, 1949

Nonionella auricula Heron-Allen and Earland, 1930

Nonionella iridea Heron-Allen and Earland, 1932

Nonionella stella Cushman and Moyer, 1930

Nonionellina labradorica (Dawson, 1860) = *Nonionina labradorica* Dawson, 1860

Nonionoides turgida (Williamson, 1858) = *Rotalina turgida* Williamson, 1858

Oolina sp. d'Orbigny, 1839

Oolina apiopleura (Loeblich and Tappan, 1953) = *Lagena apiopleura* Loeblich and Tappan, 1953

Oridorsalis umbonatus (Reuss, 1851) = *Rotalina umbonatus* Reuss, 1851

Patellina corrugata Williamson, 1858

Pullenia bulloides (d'Orbigny, 1846) = *Nonionina bulloides* d'Orbigny, 1846

Pullenia osloensis Feyling-Hanssen, 1954

Pyrgo Defrance, 1824

Quinqueloculina sp. d'Orbigny, 1826

Quinqueloculina arctica Cushman, 1933

Quinqueloculina seminula (Linnaeus, 1758) = *Serpula seminulum* Linnaeus, 1758

Reophax sp. de Montfort, 1808

Reophax scorpiurus de Montfort, 1808

Reussoolina laevis (Montagu, 1803) = *Vermiculum laeve* Montagu, 1803

Robertinoides charlottensis (Cushman, 1925) = *Robertina charlottensis* Cushman, 1925

Stainforthia concava (Höglund, 1947) = *Virgulina concava* Höglund, 1947

Stainforthia feylingi Knudsen and Sedenkrantz, 1994

Stainforthia fusiformis (Williamson, 1848) = *Bulimina fusiformis* Williamson, 1848

Stainforthia loeblichi Feyling-Hanssen, 1954

Textularia earlandi Parker, 1952

Trifarina angulosa (Williamson, 1858) = *Uvigerina angulosa* Williamson, 1858

Trifarina carinata (Cushman, 1923) = *Angulogerina carinata* Cushman, 1927

Trochammina sp. Parker and Jones, 1859

Trochammina nana (Brady, 1881) = *Haplophragmium nanum* Brady, 1881

Trochammina pseudoinflata Scott and Vilks, 1991

Veleroninoides wiesneri (Parr, 1950) = *Labrospira wiesneri* Parr, 1950

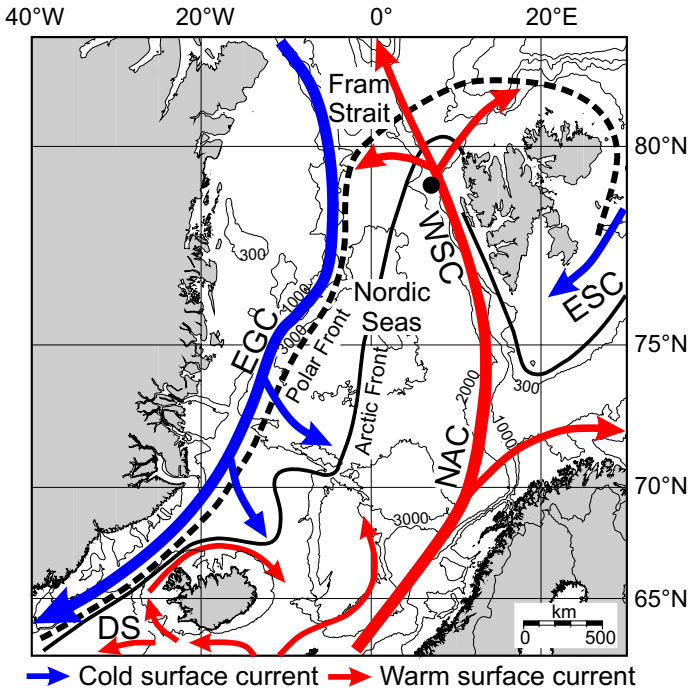
40°W
20°W
0°
20°E
80°N
75°N
70°N
65°N
Fram
Strait
MSC
ESC
EGC
Nordic
Seas
Polar Front
Arctic Front
NAC
DS
300
1000
2000
3000
km
0
500
Cold surface current
Warm surface current

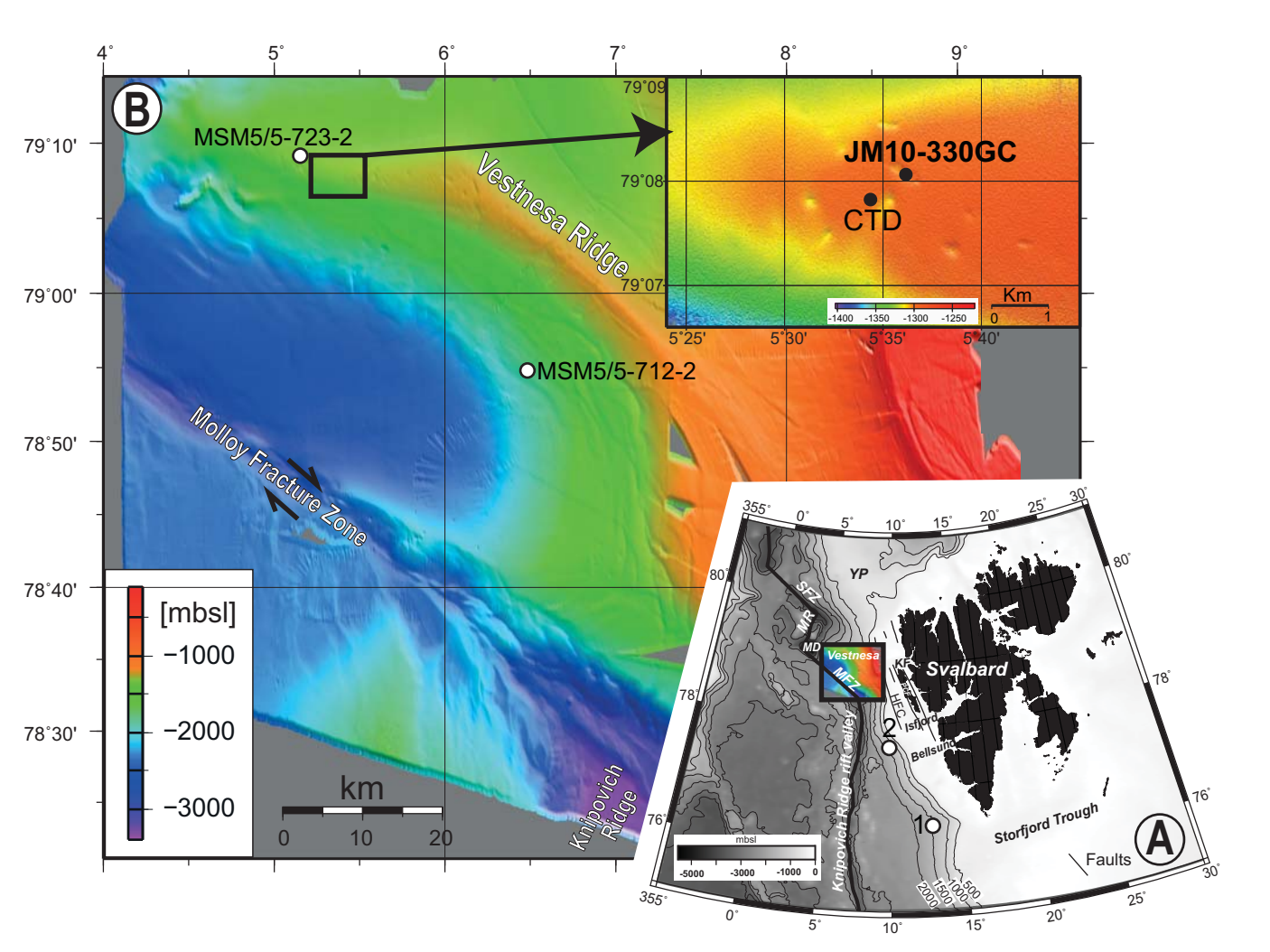
B
MSM5/5-723-2
Vestnesa Ridge
JM10-330GC
CTD
MSM5/5-712-2
Molloy Fracture Zone
Knipovich Ridge
[mbsl]
−1000
−2000
−3000
km
0 10 20
Km
0 1
-1400 -1350 -1300 -1250
4° 5° 6° 7° 8° 9°
79°10' 79°00' 78°50' 78°40' 78°30'
79°09 79°08 79°07
5°25' 5°30' 5°35' 5°40'
A
YP
SFZ
MR
MD
Vestnesa
MFZ
KF
HFC
Svalbard
Isfjorden
Bellsund
Knipovich Ridge rift valley
Storfjord Trough
Faults
1
2
mbsl
-5000 -3000 -1000 0
500
1000
1500
2000
355° 0° 5° 10° 15° 20° 25° 30°
80° 78° 76°

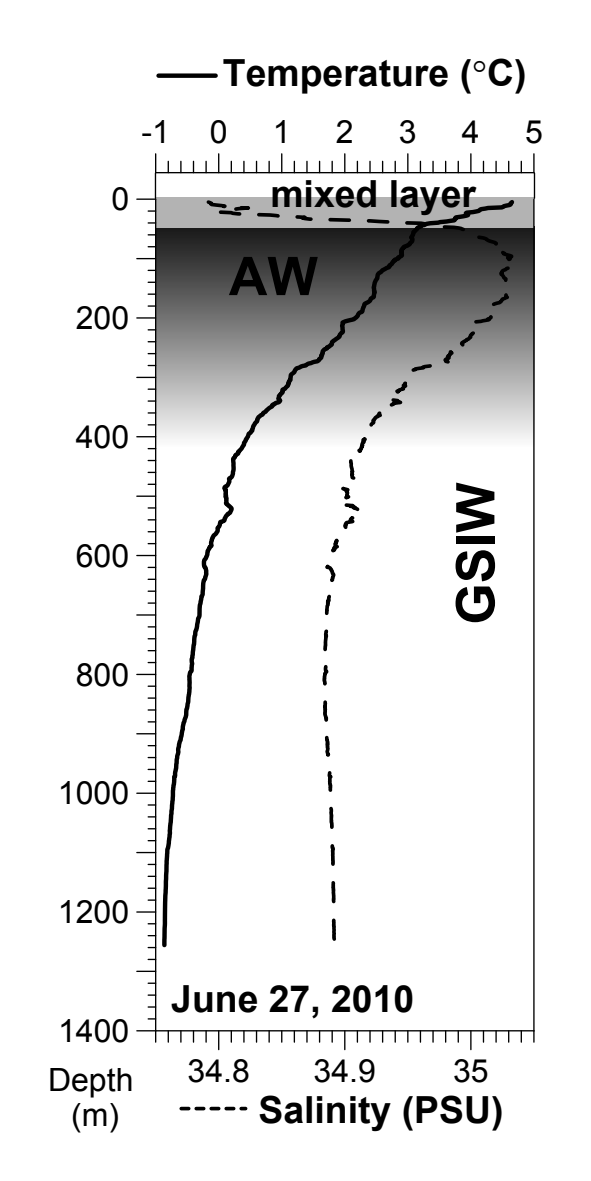
Temperature (°C)
-1
0
1
2
3
4
5
mixed layer
AW
GSIW
0
200
400
600
800
1000
1200
1400
June 27, 2010
Depth (m)
34.8
34.9
35
Salinity (PSU)

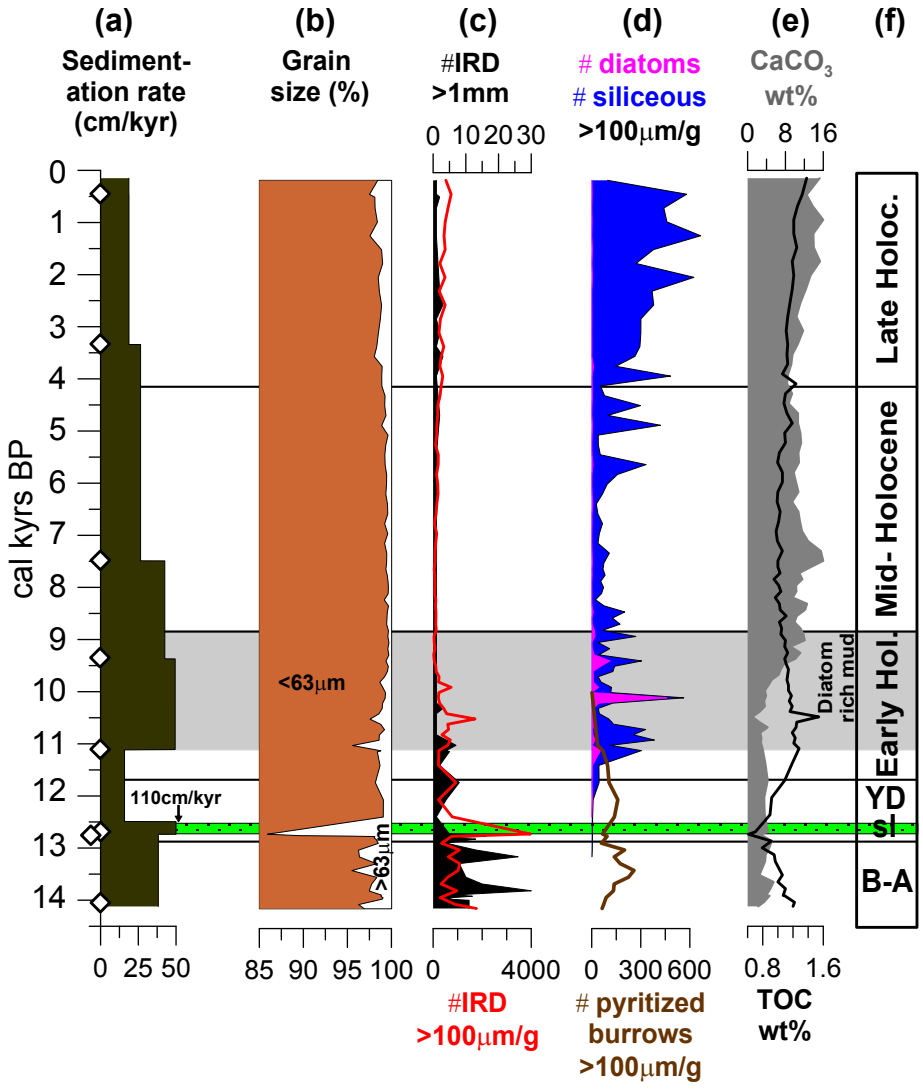
(a)
Sediment-ation rate (cm/kyr)
(b)
Grain size (%)
(c)
#IRD >1mm
(d)
diatoms
siliceous >100μm/g
(e)
CaCO3 wt%
(f)
0 10 20 30
0 8 16
cal kyrs BP
0
1
2
3
4
5
6
7
8
9
10
11
12
13
14
110cm/kyr
<63μm
>63μm
Diatom rich mud
Late Holoc.
Mid- Holocene
Early Hol.
YD
sl
B-A
0 25 50
85 90 95 100
0 4000
#IRD >100μm/g
0 300 600
pyritized burrows >100μm/g
0.8 1.6
TOC wt%

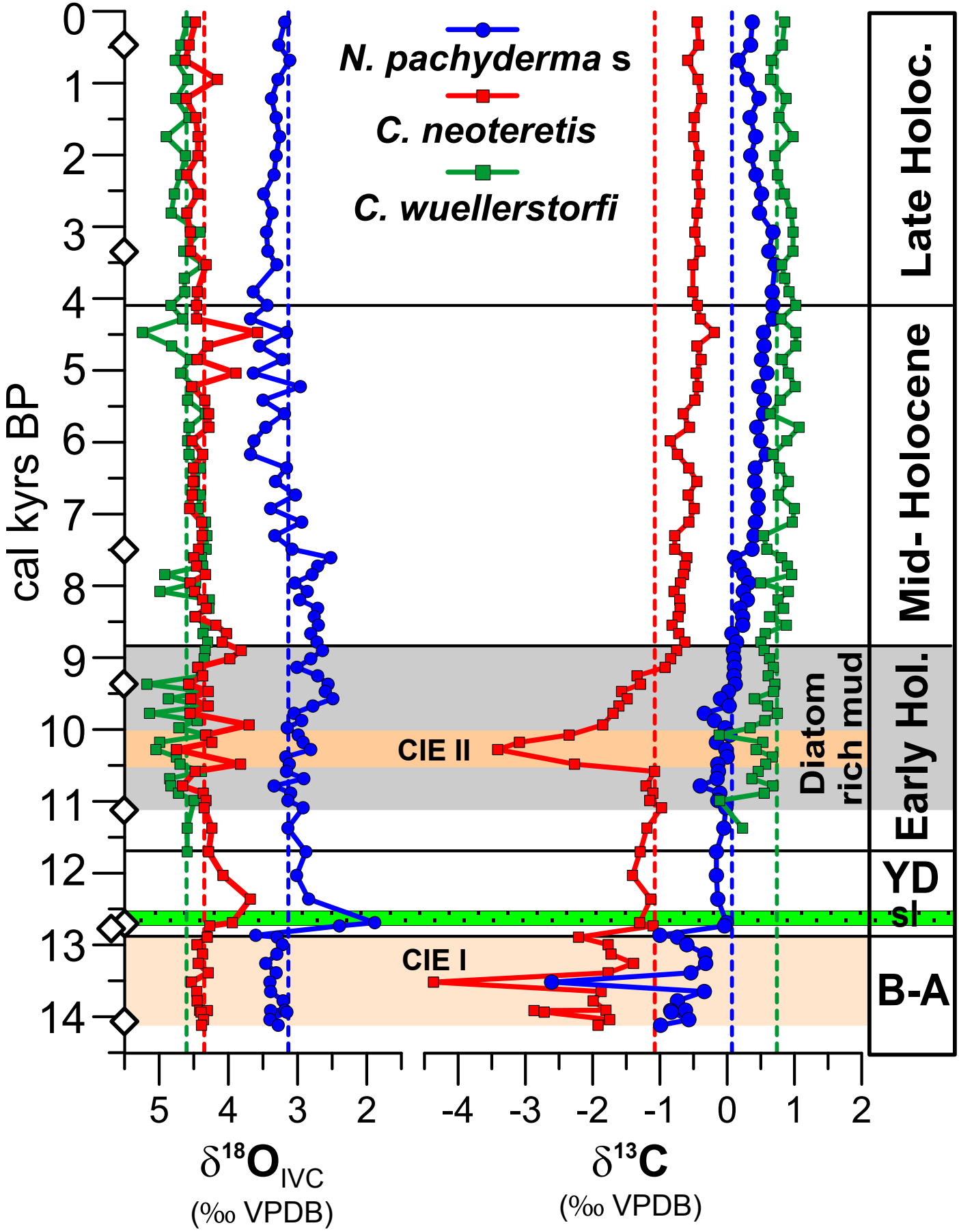
N. pachyderma s
C. neoteretis
C. wuellerstorfi
cal kyrs BP
0
1
2
3
4
5
6
7
8
9
10
11
12
13
14
Late Holoc.
Mid- Holocene
Early Hol.
YD
B-A
sl
Diatom rich mud
CIE II
CIE I
5
4
3
2
-4
-3
-2
-1
0
1
2
δ18OIVC
(‰ VPDB)
δ13C
(‰ VPDB)

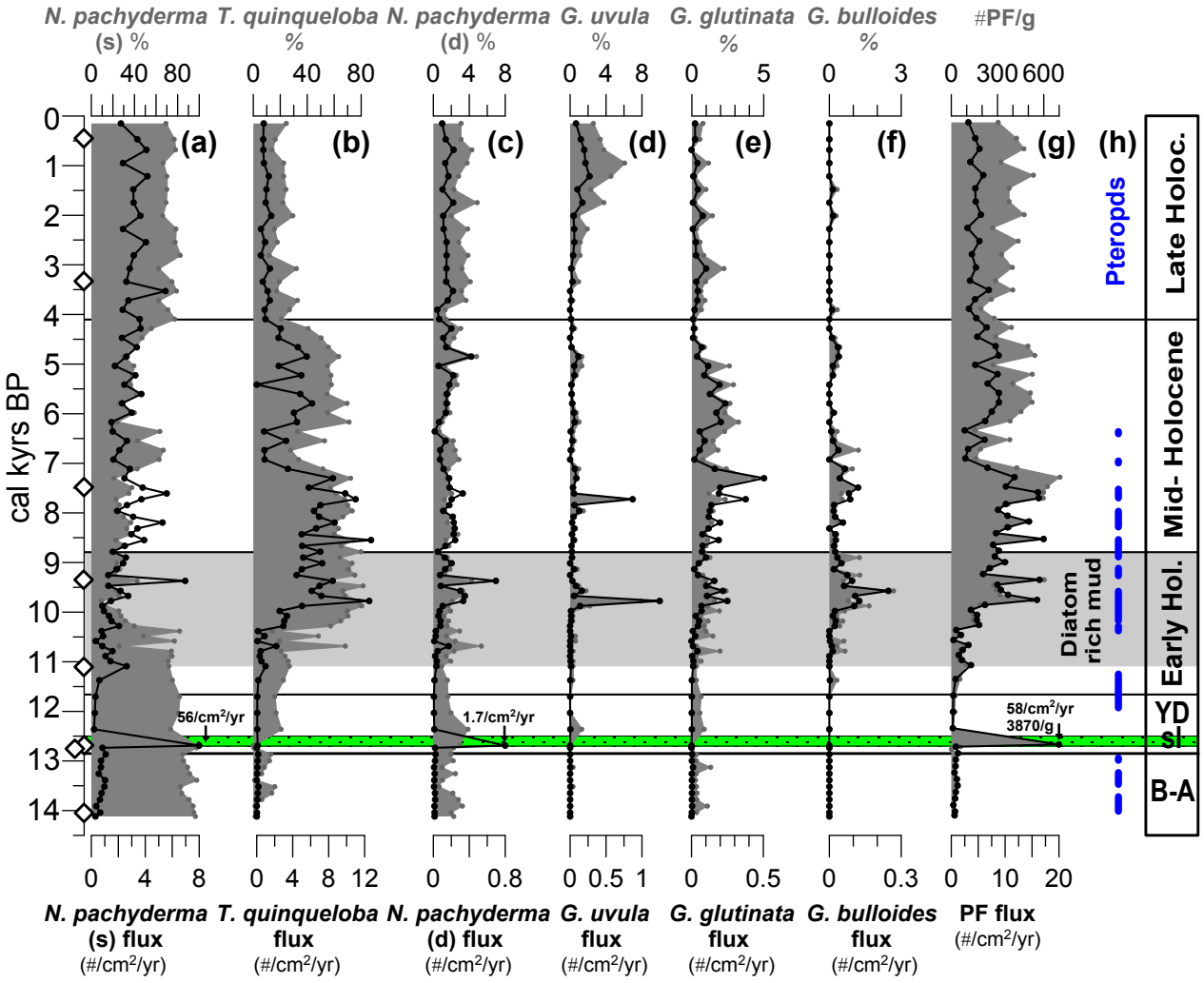
N. pachyderma (s) %
T. quinqueloba %
N. pachyderma (d) %
G. uvula %
G. glutinata %
G. bulloides %
#PF/g
(a)
(b)
(c)
(d)
(e)
(f)
(g)
(h)
Pteropds
cal kyrs BP
Late Holoc.
Mid- Holocene
Early Hol.
Diatom rich mud
YD
B-A
56/cm²/yr
1.7/cm²/yr
58/cm²/yr
3870/g
N. pachyderma (s) flux (#/cm²/yr)
T. quinqueloba flux (#/cm²/yr)
N. pachyderma (d) flux (#/cm²/yr)
G. uvula flux (#/cm²/yr)
G. glutinata flux (#/cm²/yr)
G. bulloides flux (#/cm²/yr)
PF flux (#/cm²/yr)

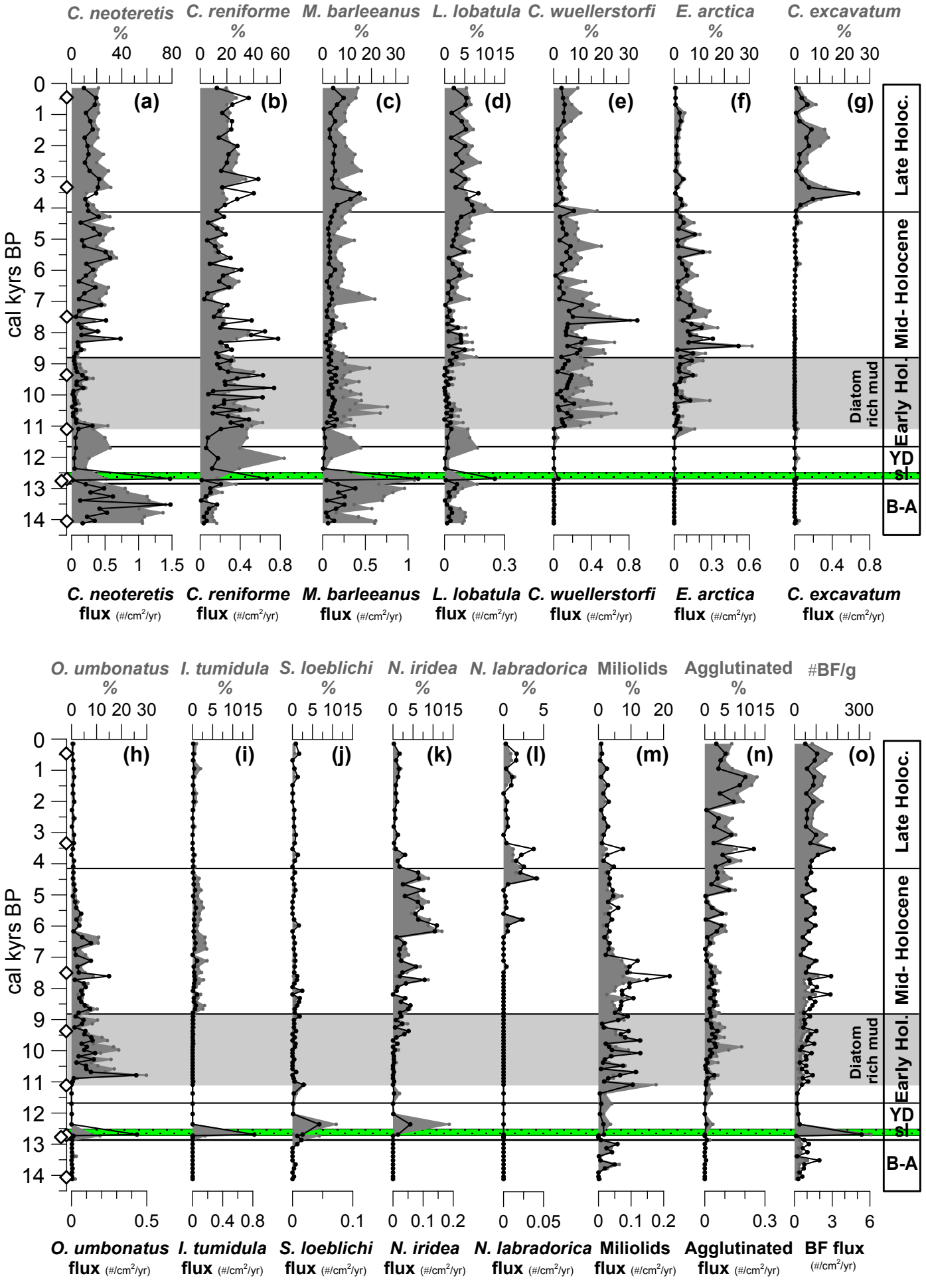
C. neoteretis
C. reniforme
M. barleeanus
L. lobatula
C. wuellerstorfi
E. arctica
C. excavatum
%
(a)
(b)
(c)
(d)
(e)
(f)
(g)
cal kyrs BP
Late Holoc.
Mid- Holocene
Early Hol.
Diatom rich mud
YD
sl.
B-A
C. neoteretis flux (#/cm²/yr)
C. reniforme flux (#/cm²/yr)
M. barleeanus flux (#/cm²/yr)
L. lobatula flux (#/cm²/yr)
C. wuellerstorfi flux (#/cm²/yr)
E. arctica flux (#/cm²/yr)
C. excavatum flux (#/cm²/yr)
O. umbonatus
I. tumidula
S. loeblichi
N. iridea
N. labradorica
Miliolids
Agglutinated
#BF/g
(h)
(i)
(j)
(k)
(l)
(m)
(n)
(o)
O. umbonatus flux (#/cm²/yr)
I. tumidula flux (#/cm²/yr)
S. loeblichi flux (#/cm²/yr)
N. iridea flux (#/cm²/yr)
N. labradorica flux (#/cm²/yr)
Miliolids flux (#/cm²/yr)
Agglutinated flux (#/cm²/yr)
BF flux (#/cm²/yr)

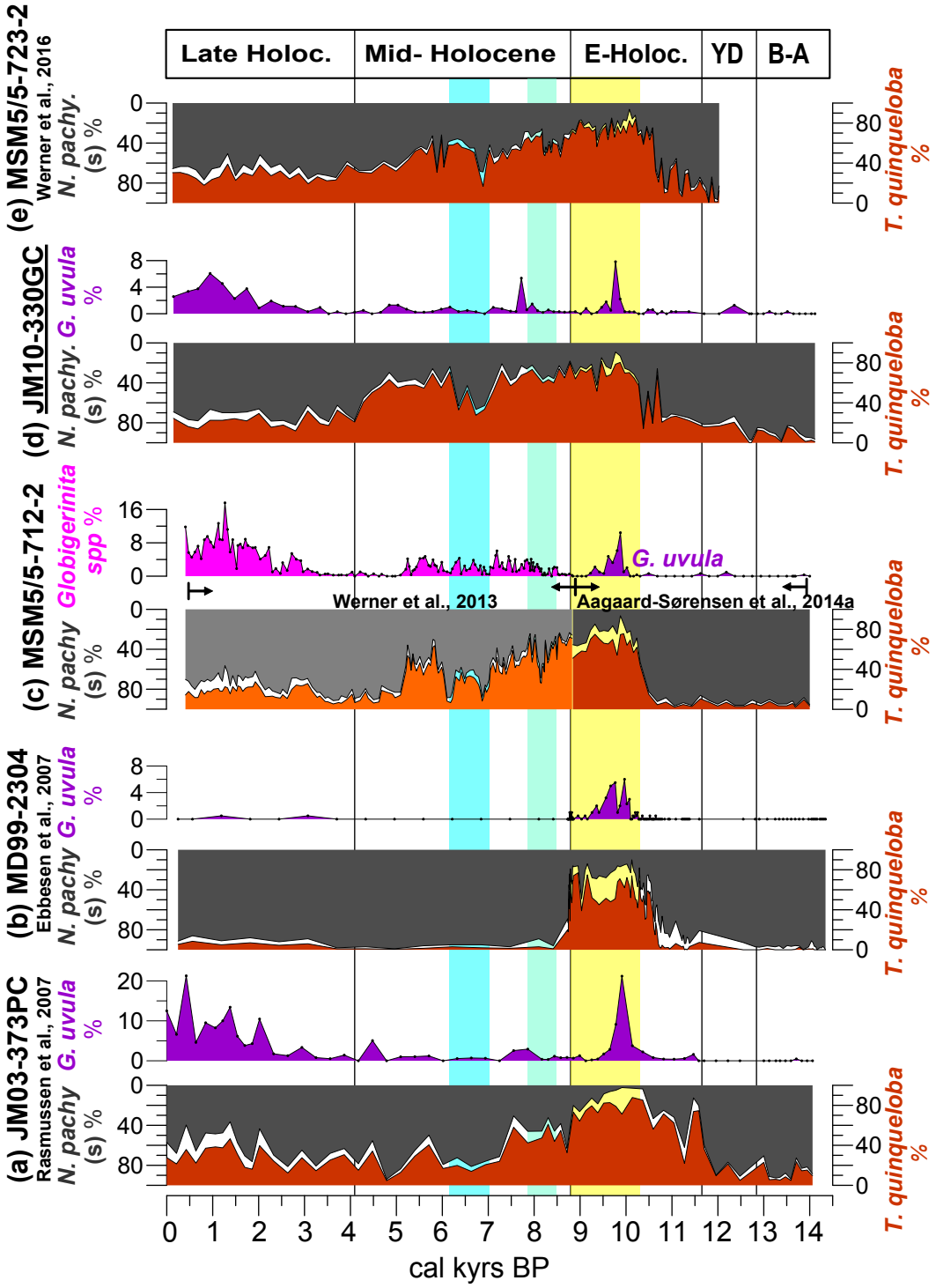
Late Holoc.
Mid- Holocene
E-Holoc.
YD
B-A
(e) MSM5/5-723-2
Werner et al., 2016
N. pachy. (s) %
T. quinqueloba %
(d) JM10-330GC
N. pachy. G. uvula (s) %
T. quinqueloba %
(c) MSM5/5-712-2
N. pachy Globigerinita spp %
G. uvula
Werner et al., 2013
Aagaard-Sørensen et al., 2014a
N. pachy (s) %
T. quinqueloba %
(b) MD99-2304
Ebbesen et al., 2007
N. pachy G. uvula (s) %
T. quinqueloba %
(a) JM03-373PC
Rasmussen et al., 2007
N. pachy G. uvula (s) %
T. quinqueloba %
cal kyrs BP

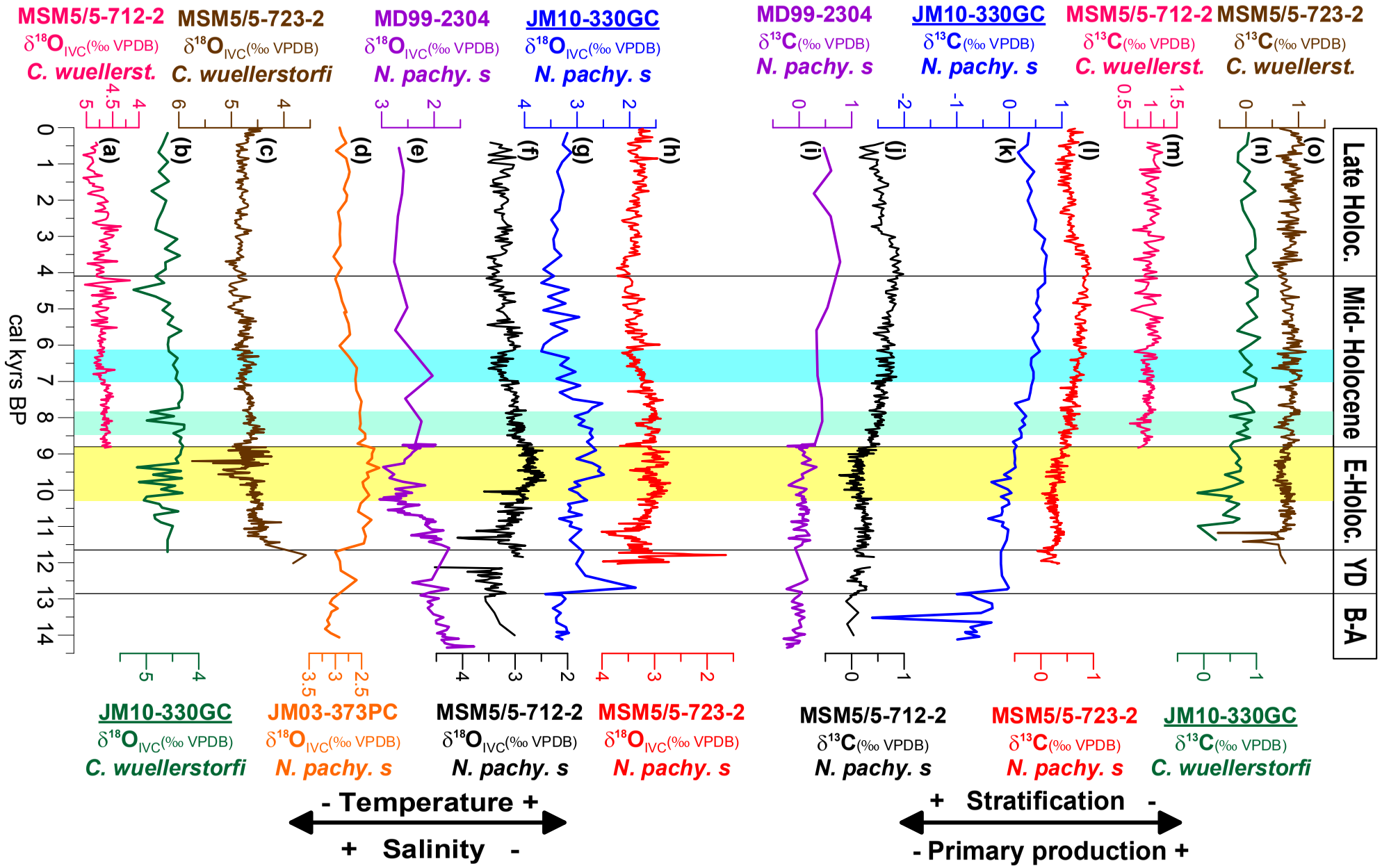
MSM5/5-712-2
δ18OIVC(‰ VPDB)
C. wuellerst.
MSM5/5-723-2
δ18OIVC(‰ VPDB)
C. wuellerstorfi
MD99-2304
δ18OIVC(‰ VPDB)
N. pachy. s
JM10-330GC
δ18OIVC(‰ VPDB)
N. pachy. s
MD99-2304
δ13C(‰ VPDB)
N. pachy. s
JM10-330GC
δ13C(‰ VPDB)
N. pachy. s
MSM5/5-712-2
δ13C(‰ VPDB)
C. wuellerst.
MSM5/5-723-2
δ13C(‰ VPDB)
C. wuellerst.
cal kyrs BP
Late Holoc.
Mid- Holocene
E-Holoc.
YD
B-A
JM10-330GC
δ18OIVC(‰ VPDB)
C. wuellerstorfi
JM03-373PC
δ18OIVC(‰ VPDB)
N. pachy. s
MSM5/5-712-2
δ18OIVC(‰ VPDB)
N. pachy. s
MSM5/5-723-2
δ18OIVC(‰ VPDB)
N. pachy. s
MSM5/5-712-2
δ13C(‰ VPDB)
N. pachy. s
MSM5/5-723-2
δ13C(‰ VPDB)
N. pachy. s
JM10-330GC
δ13C(‰ VPDB)
C. wuellerstorfi
- Temperature +
+ Salinity -
+ Stratification -
- Primary production +

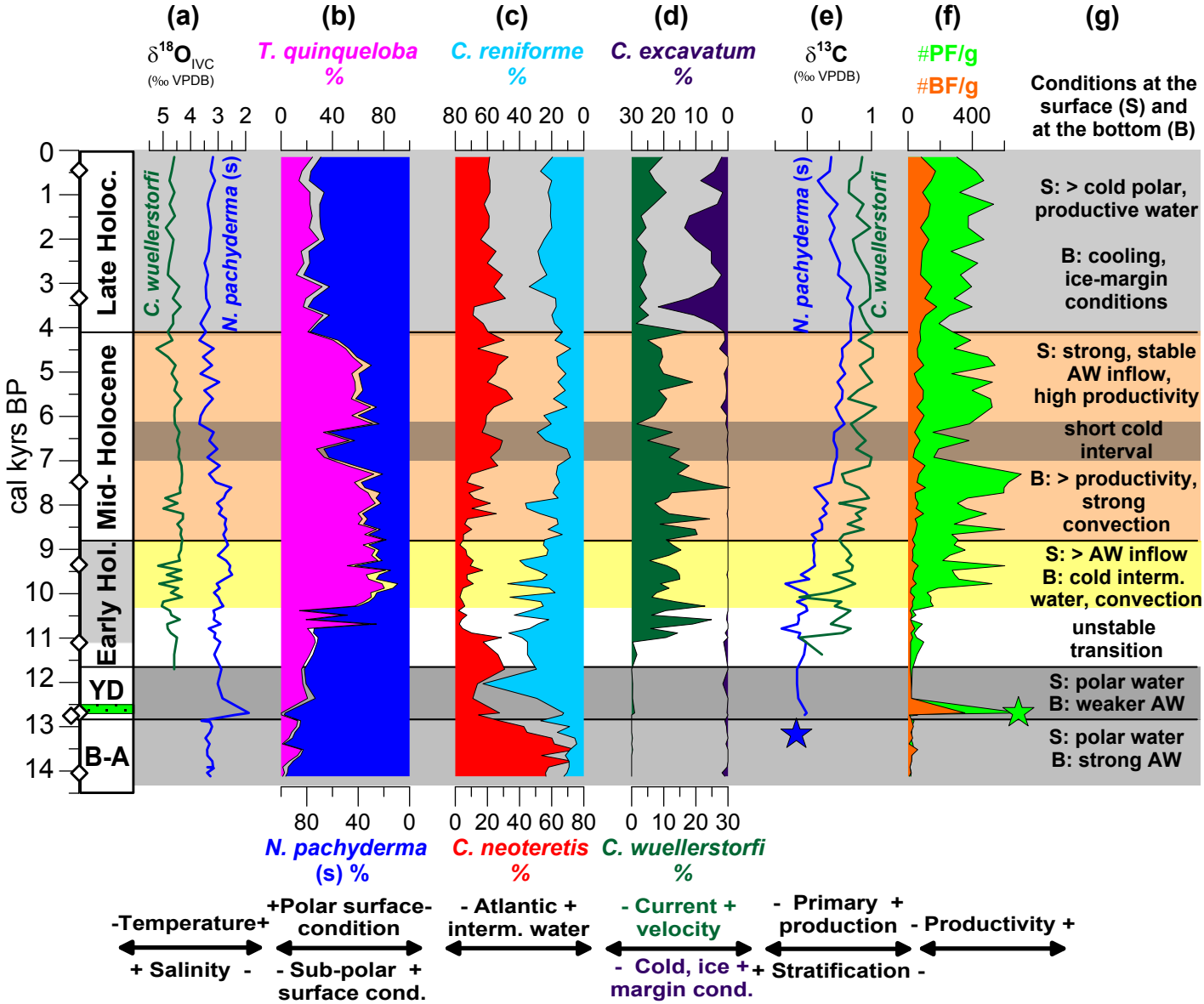
(a)
δ18OIVC (‰ VPDB)
5 4 3 2
C. wuellerstorfi
N. pachyderma (s)
(b)
T. quinqueloba %
0 40 80
(c)
C. reniforme %
80 60 40 20 0
(d)
C. excavatum %
30 20 10 0
(e)
δ13C (‰ VPDB)
0 1
N. pachyderma (s)
C. wuellerstorfi
(f)
#PF/g
#BF/g
0 400
(g)
Conditions at the surface (S) and at the bottom (B)
cal kyrs BP
0 1 2 3 4 5 6 7 8 9 10 11 12 13 14
Late Holoc.
Mid- Holocene
Early Hol.
YD
B-A
S: > cold polar, productive water
B: cooling, ice-margin conditions
S: strong, stable AW inflow, high productivity
short cold interval
B: > productivity, strong convection
S: > AW inflow
B: cold interm. water, convection
unstable transition
S: polar water
B: weaker AW
S: polar water
B: strong AW
80 40 0
N. pachyderma (s) %
0 20 40 60 80
C. neoteretis %
0 10 20 30
C. wuellerstorfi %
-Temperature+
+ Salinity -
+Polar surface-condition
- Sub-polar + surface cond.
- Atlantic + interm. water
- Current + velocity
- Cold, ice + margin cond.
- Primary + production
+ Stratification -
- Productivity +

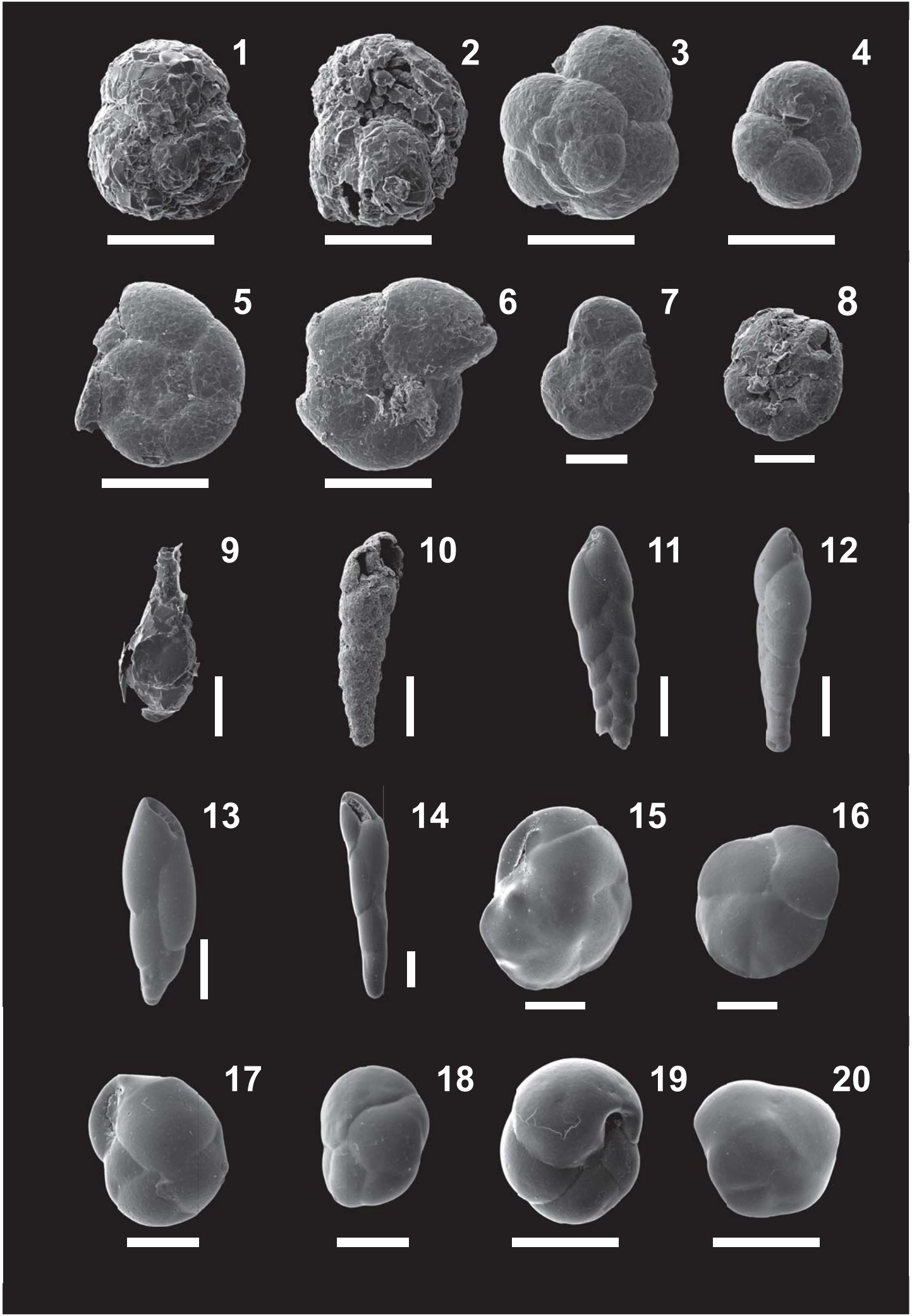
1
2
3
4
5
6
7
8
9
10
11
12
13
14
15
16
17
18
19
20

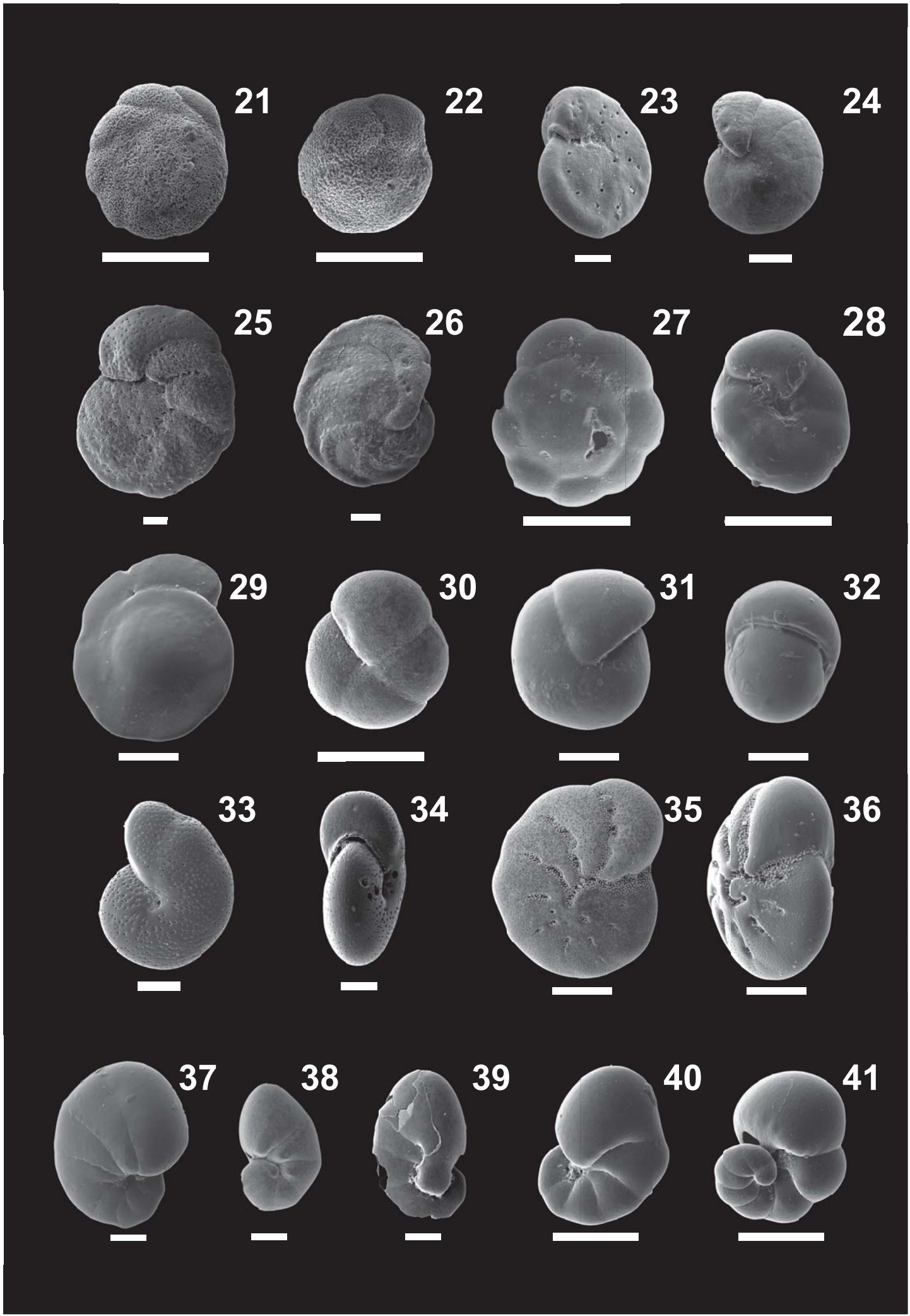
21
22
23
24
25
26
27
28
29
30
31
32
33
34
35
36
37
38
39
40
41